Federal Policy Research

Final report

DETECTION OF OZONE RECOVERY IN THE ARCTIC | DORA

RT/23/DORA

Corinne Vigouroux – Royal Belgian Institute for Space Aeronomy (BIRA-IASB)
Caroline Jonas – Royal Belgian Institute for Space Aeronomy (BIRA-IASB)

Federal Policy Research

Final report

DETECTING OZONE RECOVERY IN THE ARCTIC | DORA

RT/23/DORA

PROMOTORS: Corinne Vigouroux (BIRA-IASB)

AUTHORS: Caroline Jonas (BIRA-IASB)
Corinne Vigouroux (BIRA-IASB)

Published in 2026 by the Belgian Science Policy Office
WTCIII
Simon Bolivarlaan 30 bus 7
Boulevard Simon Bolivar 30 bte 7
B-1000 Brussels
Belgium
Tel: +32 (0)2 238 34 11
http://www.belspo.be
https://www.belspo.be/belspo/IMPULS/index_en.stm

Contact person: Corinne Vigouroux
Tel: +32 (0)2 237 3367
Corinne.vigouroux@aeronomie.be

Neither the Belgian Science Policy Office nor any person acting on behalf of the Belgian Science Policy Office is responsible for the use which might be made of the following information. The authors are responsible for the content.

No part of this publication may be reproduced, stored in a retrieval system, or transmitted in any form or by any means, electronic, mechanical, photocopying, recording, or otherwise, without indicating the reference:

Corinne Vigouroux and Caroline Jonas. ***Detection of ozone recovery in the Arctic***. Final Report. Brussels: Belgian Science Policy Office 2026 – 49 p. Federal Policy Research

TABLE OF CONTENTS

ABSTRACT 5
1. INTRODUCTION 6
2. MOTIVATION AND OBJECTIVES OF THE OBJECTIVES 7
3. METHODOLOGY 9
4. SCIENTIFIC RESULTS AND RECOMMENDATIONS 19
5. DISSEMINATION AND VALORISATION 38
6. PUBLICATIONS 40
7. ACKNOWLEDGEMENTS 41
ANNEXES 42

ABSTRACT

Context

Contrary to the Antarctic, where ozone recovery has been observed for about a decade, the detection of positive ozone trends in the Arctic remains challenging due to higher natural variability of ozone in that region. The trends are expected to be small (few percent/decade) which complicates their detection. **This project aims to explore if the ozone recovery in the Arctic can be detected using long-term ground-based observations by reducing the uncertainty on the trends.**

Objectives

Reducing the uncertainty on the trends will be obtained through three objectives:

- **Select the best quality ground-based time series in Arctic**. Ground-based measurements are cross-compared to two satellite data sets (MEGRIDOP and IASI-CDR). This enables the detection of drifted ground-based data sets we further exclude from our study.

- Use a representativeness study based on CAMS re-analysis data to define regions representative of the same ozone variability. This allows **the merging of data sets from different instruments and stations**, which reduces the noise in the time-series and increases their sampling.

- Annual and seasonal **trends are calculated using a multiple linear regression (MLR)** technique involving a set of proxies that represent physical processes influencing the natural ozone variability, reducing the remaining variability in the time-series. The MLR also allows the ozone variability associated with each included process to be quantified. The remaining stratospheric ozone trend can then be mostly attributed to the reduction of ODS and quantified.

Conclusions

We succeeded to detect significant ozone recovery in some regions of the Arctic: over Canada and Reykjavik (+2.1 %/decade) and North-West Europe (Harestua and Lerwick, +0.7 %/decade). Ozone recovery is also observed over Canada in the mid-stratosphere (+2.0 %/decade) and over the North Pole region (Canada and Ny-Ålesund) in the upper stratosphere (+2.1 to +3.8 %/decade). By analysing the sensitivity of the ozone trends to the proxies, we observe a slow-down of the expected ozone recovery, especially in the lower stratosphere, due to stratospheric cooling (-0.6 %/decade) and to the increase of volume of polar stratospheric clouds (-0.8 %/decade).

Our findings are currently published in preprint in ACP: EGUsphere [preprint], https://doi.org/10.5194/egusphere-2025-6473

Keywords

Ozone trends, Arctic, Ground-based measurements

1. INTRODUCTION

Belgium, and in particular the Royal Belgian Institute for Space Aeronomy (BIRA), has a **strong involvement in international research initiatives focusing on long-term ozone trends**: 1) the **LOTUS** initiative (Long-term Ozone Trends and Uncertainties in the Stratosphere) within SPARC (Stratosphere-troposphere Processes and their Role in Climate) which results are used extensively in the WMO (World Meteorological Organization) Scientific Assessments of Ozone Depletion, and 2), the **TOAR** initiative (Tropospheric Ozone Assessment Reports) within IGAC (International Global Atmospheric Chemistry). We propose to **strengthen our position in these initiatives by focusing on the Arctic**, which is currently **far less explored in LOTUS and TOAR**, compared to the tropical and mid-latitude.

Thanks to the Montreal Protocol and its Adjustments and Amendments to reduce the emissions of ozone depleting substances (ODS), **stratospheric ozone is expected to slowly recover globally, although the delay of the recovery is still unsure due to the uncertainties associated to climate change**. Detecting this recovery is very challenging because of the large natural variability of stratospheric ozone, and the expected small trend (a few percent per decade). In the polar regions, ozone is especially highly impacted by the effective-chlorine levels, which leads to the well-known "ozone hole" problematic. It is therefore expected that it is easier in the polar regions to detect the recovery of ozone attributed to the decrease of effective chlorine. Indeed, there are early signs of ozone recovery observed in Antarctica (WMO, 2018). However, the much **higher ozone natural variability in the Arctic, due to larger dynamical variability, complicates the observation of the ozone recovery in the Arctic and no evidence of positive ozone trends over the Arctic was found for the 2000-2016 period** (WMO 2018).

2. MOTIVATION AND OBJECTIVES OF THE PROJECT

This project aims to explore if the ozone recovery in the Arctic can be detected using long-term ground-based observations by reducing the uncertainty on the trends.

Reducing the uncertainty on the trends will be obtained through three objectives:

First objective: Select the best quality ground-based time series in Arctic.

Our first focus is Fourier Transform Infra-Red (FTIR) data with which our team has a strong expertise, especially in its capability to be used for detecting ozone trends and variability (Vigouroux et al., 2008, 2015). We use the NDACC (Network for the Detection of Atmospheric Composition Change) public data from seven FTIR sites, located at latitudes from 60 to 80°N. FTIR measurements provide total columns as well as independent partial columns in the troposphere and stratosphere. In addition, we use ozone soundings (troposphere and stratosphere) and Brewer and Dobson spectrometers (total columns) in the Arctic.
We had in our proposal the objective **of using our Arctic ground-based data sets to evaluate ozone trends from satellites** (which are usually merged satellite data sets for long-term trend studies). Satellite measurements usually have larger uncertainties over polar regions, and there is a **strong need to assess their long-term stability, and to verify that the merging does not introduce some step or drifts in the long-term data sets**. We would like to detect possible drifts in the recent merged Limb satellite data set that were optimized during the LOTUS/SPARC initiative (MEGRIDOP, Sofieva et al., 2021), and IASI-CDR Nadir total columns and profiles from AERIS L3 products (Clerbaux and Coheur 2025a, 2025b, Keppens 2025). It was found in the TOAR initiative that the tropospheric trends from satellites do not agree, IASI being the only record showing negative trends (Gaudel et al., 2018), which highlights the need for validation of the new version of IASI.

It turned out that we can, in addition, use these two satellite data sets to identify some ground-based time-series that are outliers in terms of drifts with both satellites.

Second objective: Use a representativeness study based on CAMS re-analysis data to define regions representative of the same ozone variability.
An obvious limitation of ground-based observations for detecting and quantifying ozone trends is the representativeness of these sparse data: **Are the detected trends at a specific site representative for ozone behavior at a regional scale?** Is the current network of ground-based stations (all long-term FTIR, Brewer, Dobson, and ozonesonde time series available in the Arctic) representative of ozone trends in the Arctic? Our second objective will be to answer these questions by using CAMS (Copernicus Atmosphere Monitoring Service) reanalysis over the Arctic. The CAMS data, combining model data and satellite observations (via data assimilation), may not be reliable for long-term trend estimation but they provide a good estimate of the ozone variability on short-time scales, which is essential to study the representativeness. For each station in the Arctic, we will provide correlation maps between CAMS output at the location of that station and CAMS data for the rest of the Arctic. **For the sites that are found representative of the same area in the Arctic, we will construct merged time series of ozone anomalies and we will obtain regional trends, which will reduce trend uncertainties thanks to reduced variability and higher sampling.**

Third objective: use a multiple linear regression (MLR) to reduce further trend uncertainty and explain ozone variability

The detection and attribution of the long-term ozone trends will be accomplished through the multiple linear regression (MLR) technique involving a set of proxies that represent physical processes influencing the natural ozone variability (e.g. solar cycle, Quasi Biennial Oscillation, Arctic Oscillation,…). The idea behind this technique is to reduce the uncertainty of the derived trends by diminishing the unexplained ozone variability, which is important because of the expected small trends compared to natural variability. The MLR also allows the ozone variability associated with each included process to be quantified. The remaining stratospheric ozone trend can then be mostly attributed to the reduction of ODS and quantified.

In addition, and **in relation to the TOAR activities**, we will determine the tropospheric trends at the same regions. **As tropospheric ozone is one of the most important greenhouse gases, it is crucial to monitor it and detect its trend in the Arctic environment which is warming at least three times faster than the rest of the globe** (IPCC Sixth Assessment report, 2021).

The consistency between the observed total and stratospheric ozone trends is currently missing or at least incomplete in ozone research (WMO 2018, chapter 3, Scientific summary and Sect. 3.3.2.4). We will address this by studying the impact of tropospheric ozone trends on the total ozone trends.

3. METHODOLOGY

SECTION A: DESCRIPTION OF DATASETS

We use data from 17 different stations, all located between 60º and 90º N (see Figure 1) and from four different ground-based instrument techniques: Fourier transform infrared (FTIR) interferometers, ozonesondes, Brewer and Dobson spectrophotometers. Simultaneous use of these techniques enables to cover the whole stratosphere and troposphere layers: FTIR, Brewer and Dobson provide total columns of ozone, ozonesondes yield high-resolution profiles up to about 30 km, and four partial columns (one in the troposphere and three in the stratosphere) can additionally be extracted from FTIR.

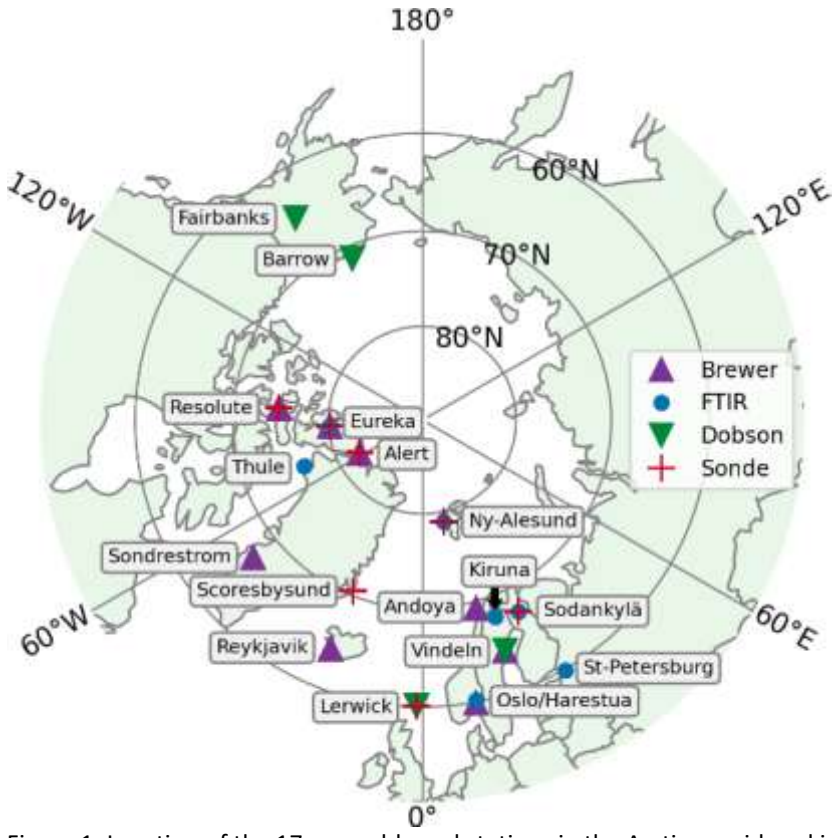

Figure 1: Location of the 17 ground-based stations in the Arctic considered in this study.

FOURIER TRANSFORM INFRARED (FTIR) SPECTROMETERS:

The FTIR interferometers record interferograms from sunlight that are Fourier-transformed into solar absorption spectra. Trace gas abundances, such as ozone abundances are retrieved from these spectra by using line-by-line spectral fitting softwares, SFIT4 (Hannigan et al. 2024) or PROFITT, including radiative transfer models (e.g. Hase et al., 2004). Forward model inputs include spectroscopic parameters, climatological a priori information on trace gases concentrations, and 6-hourly pressure, temperature profile information from NCEP. The pressure and temperature-dependence of the ozone line-shapes enable us to retrieve low-vertical resolution profiles, with four to five distinct degrees of freedom for signal (DOFS), spanning the troposphere and stratosphere from about $0-48$ km (Vigouroux et al. 2015). In this study we use FTIR ozone datasets from the Network for the Detection

of Atmospheric Composition Change (NDACC). This network gathers datasets of 160 ground-based instruments monitoring various components of the atmosphere from 73 active sites around the globe. It represents a massive collaborative effort lasting for about 35 years now, enabling detection of long-term trends, validation of other datasets and model datasets (De Mazière et al. 2018). There are six NDACC FTIR instruments within the Arctic: Ny-Ålesund, Eureka, Kiruna, Harestua, St Petersburg and Thule, see Table 2. These instruments are Bruker high-resolution ($< 0.005\text{cm}^{-1}$) spectrometers. The retrieval strategy used at all these sites is standardized by the InfraRed Working Group (IRWG) (IRWG 2025). It has been recently updated from the previous version described in details in (Vigouroux et al. 2015) to an improved strategy (IRWG2023), based on the HITRAN2020 molecular spectroscopic database (Gordon et al. 2022), specific spectral microwindows (around $1000\,\text{cm}^{-1}$) fitted to avoid interference with water vapor lines, an updated regularization scheme (Tikhonov) and an updated a priori (WACCMv7 IRWG (IRWG 2025)). More details on this new strategy used here can be found in the appendix of (Björklund et al. 2024), where it was found to reduce biases with other instruments in Lauder, New Zealand from $1-3\%$ for all partial columns as well as to reduce drifts.

In addition, we consider a new ozone time-series that we have obtained by applying a new retrieval (in the $3040\,\text{cm}^{-1}$ region following the strategy of (Zhou et al. 2020) and (García et al. 2014)) to spectra recorded by the Sodankylä instrument that is part of the Total Carbon Column Observing Network (TCCON). The resulting vertical profiles contain lower DOFS of about 2.5, concentrated on the stratospheric layers, see Table 1.

For all time-series, the uncertainty on ozone partial columns is obtained from the propagation of the retrieved profile uncertainties, while random and systematic uncertainties are themselves obtained using optimal estimation (Rodgers 2000; Vigouroux et al. 2015). The random error of partial columns additionally contains a smoothing error (Rodgers 2000) estimated from the WACCMv7 covariance matrix at each site. In Table 1 we provide the mean of the obtained uncertainties in percent for each partial column considered in this paper and the total column of ozone (TCO). The partial columns are based on FTIR DOFS that are explicitly given here for NDACC products and for the Sodankylä product.

	Rand.	Syst.	Total	DOFS NDACC	DOFS Sod.
0-8km	5.43	6.19	8.57	0.89	0.07
8-17km	3.49	4.27	5.77	1.04	0.72
10-17km	4.26	4.15	6.27	0.89	0.67
17-26km	3.30	4.10	5.40	1.06	0.92
26-48km	3.87	6.35	7.53	1.20	0.68
32-48km	6.68	8.61	11.03	0.82	0.24
TCO	1.38	3.46	3.80	4.39	2.38

Table 1: Mean FTIR random, systematic and total uncertainties in percent and average DOFS of NDACC FTIR and of Sodankylä FTIR for each partial column and the total column of ozone (TCO).

OZONESONDES:

Ozonesondes are small, light-weight devices flown on weather balloons that measure the vertical profile of ozone based on the titration of ozone in a neutral buffered potassium iodide sensing solution, with a precision better than $\pm(3-5)\%$ and an accuracy of about $\pm(5-10)\%$ for up to 30 km altitude (Smit et al. 2024). However, changes in preparation and operation procedures, manufacturer type, sensing solution strength, and processing might result in biases in the time-series, compromising any reliable ozone trends assessment. Therefore, a homogenization activity, correcting for those biases following recommendations in (Smit and ASOPOS 2.0 Panel 2021; Smit and O3S-DQA Panel 2012) has been undertaken, with all the homogenized ozonesonde data stored and described

within the framework of the Tropospheric Ozone Assessment Report Phase II (TOAR-II) Focus Working Group HEGIFTOM (Harmonization and Evaluation of Ground-based Instruments for Free-Tropospheric Ozone Measurements, see also (Van Malderen, Thompson, et al. 2025)). In this study, the data from the Canadian Arctic sites Resolute, Alert, and Eureka and the European Arctic sites Scoresbysund, Ny-Ålesund, Sodankyla and Lerwick have been used. More details on the specific homogenization steps needed to correct those datasets are provided in (Tarasick et al. 2016) for Resolute, Alert, and Eureka and in (Nilsen et al. 2024) for Scoresbysund, Ny-Ålesund, and Sodankylä.

We have capped sondes profiles at 26 km so that the mid stratospheric column contains at least 60% of all measured profiles at all sites (in some sites such as Alert and Resolute, less than 50 to 40% of profiles reach up to 30 km because the sondes balloon burst before that altitude). Extreme outliers are found in the data after summing the profiles into partial columns. They are removed by applying a very loose percentile filter: for q_1 and q_3 the 25th and 75th percentiles, we remove datapoints lying beyond $q_3 + 8(q_3 - q_1)$ or below $q_1 - 8(q_3 - q_1)$ for each partial column time-series.

BREWER AND DOBSON SPECTROPHOTOMETERS:

Brewer and Dobson spectrophotometers use UV light (about 350nm) to extract the total column of ozone by comparing relative intensities for pairs of selected wavelengths. All Brewer and Dobson total column datasets used in this study are obtained from the World Ozone and Ultraviolet Radiation Data Centre (WOUDC) repository (...). We use Brewer total column measurements from Resolute, Sondrestrom, Alert, Eureka, Vindeln, Oslo, Andoya and Dobson total column measurements from Lerwick, Barrow, Reykjavik, Fairbanks and Vindeln. They are given as daily measurements obtained from several measurements averaged together with a standard deviation measure. When the standard deviation is not provided, we use a generic random error of 1% for direct sun observation (DS) and 5% for other types of measurement (zenith-sun ZS, focused-moon FM), see (Fioletov et al. 2005; Vogler et al. 2007). The Brewer in Alert has calibration issues concerning ZS measurements so these are excluded from the dataset. For all Brewer measurements we restrict to airmass factors $\mu < 3.5$ for single monochromator instruments (MKII, MKIV and MKV). Finally, most stations have measurements taken by several instruments. In that case we average all same-day observations with a weighted mean.

Site	Lat.ºN	Lon.	Instr.	Repository	Time period
Alert	82.49	62.34ºW	Sonde	Hegiftom	$2000-2024$
			Brewer	WOUDC	$2004-2024$
Eureka	80.10	86.40ºW	FTIR	NDACC	$2006-2020$
			Brewer	WOUDC	$2001-2024$
Ny-Ålesund	78.92	11.92ºE	FTIR	NDACC	$2000-2024$
			Sonde	Hegiftom	$2000-2024$
Thule	76.52	68.77ºW	FTIR	NDACC	$2000-2024$
Resolute	74.70	94.96ºW	Sonde	Hegiftom	$2000-2024$*
			Brewer	WOUDC	$2000-2024$
Barrow	71.30	156.60ºW	Dobson	WOUDC	$2000-2024$
Scoresbysund	70.48	21.97ºW	Sonde	Hegiftom	$2000-2024$†
Andoya	69.28	62.34ºW	Brewer	WOUDC	$2000-2024$
Kiruna	67.84	20.41ºE	FTIR	private	$2000-2022$

Site	Lat.ºN	Lon.	Instr.	Repository	Time period
Sodankyla	67.37	26.63ºE	FTIR	BIRA-IASB	2012 – 2024
			Sonde	Hegiftom	2000 – 2024
Sondrestrom	66.99	50.95ºW	Brewer	WOUDC	2000 – 2023
Fairbanks	64.90	147.90ºW	Dobson	WOUDC	2000 – 2024
Vindeln	64.24	19.77ºE	Dobson	WOUDC	2000 – 2024
			Brewer	WOUDC	2000 – 2024
Reykjavik	64.13	21.90ºW	Dobson	WOUDC	2000 – 2024
Harestua	60.20	10.80ºE	FTIR	NDACC	2000 – 2024
Oslo	59.94	10.72ºE	Brewer	WOUDC	2000 – 2024
Lerwick	60.13	1.18ºW	Sonde	Hegiftom	2000 – 2024
			Brewer	WOUDC	2000 – 2024
St Petersburg	59.90	29.80ºE	FTIR	NDACC	2009 – 2024

Table 2: Summary of all the ground-based data sets that have been considered in this study ordered by decreasing latitude. * Resolute's is restricted to the 2005–2024 time period as explained in the result section, in "Validation of ground-based datasets using satellites". †Scoresbysund's time series is not used at all in the trend analysis for reasons detailed in the same result section.

CHOICE OF PARTIAL COLUMNS AND ANOMALIES DEFINITION

While Dobson and Brewer datasets only provide a total column measurement of the ozone abundance, ozonesondes and FTIR present vertically resolved profiles. Since this vertical resolution only contains four to five degrees of freedom for the FTIR, we divide the troposphere and stratosphere into four layers (see Table 3) to obtain four partial columns of ozone, each containing about one DOFS for the FTIR (see Table 2). The specific choice of boundaries for these layers reflects the need for merging FTIR with sondes datasets.

	Troposphere	Lower stratosphere	Mid stratosphere	Upper stratosphere	Total column
Layer (km)	0 – 8	8 – 17	17 – 26	26 – 48	0 – 60
CAMS grid	1000 – 300 hPa	300 – 100 hPa	100 – 20 hPa	20 – 1 hPa	TC
Datasets used	FTIR* Sondes	FTIR Sondes	FTIR Sondes	FTIR	FTIR* Brewer Dobson

Table 3: Altitude layers defining the four partial columns of ozone considered for ozonesondes and FTIR. Partial columns are calculated from profiles using the altitude in kilometers. The CAMS grid line reports the approximate equivalent pressure layers used for calculating partial columns of CAMS data in the representativeness study (see section 4). The last line summarizes which datasets are used in each partial column of this study. The asterisk next to FTIR means that the lower-resolution product at Sodankylä is excluded.

During winter, the tropopause in the Arctic typically lies at 8 km, but this value can become larger with seasons. To ease comparison to satellite products (MEGRIDOP Limb profiles only starts from 10 km), we will consider an alternative lower stratospheric column from $10-17$ km when comparing ground-based to satellite datasets. Moreover, we additionally consider a second upper stratospheric column from $32-48$ km when calculating ozone trends.

From those ozone columns we first calculate daily mean time-series, and from those we obtain monthly mean time-series. We then use the monthly mean time-series to calculate relative (1) and absolute (2) anomalies:

$$\mathrm{anom}^{\mathrm{month}_x,\mathrm{year}_y} = \frac{O_3^{\mathrm{month}_x,\mathrm{year}_y} - O_3^{\mathrm{month}_x}}{O_3^{\mathrm{month}_x}}; \qquad (1)$$

$$\mathrm{abs.anom}^{\mathrm{month}_x,\mathrm{year}_y} = O_3^{\mathrm{month}_x,\mathrm{year}_y} - O_3^{\mathrm{month}_x}; \quad (2)$$

with

$$O_3^{\mathrm{month}_x} = \frac{1}{n+1}\sum_{y=\mathrm{start\ year}}^{\mathrm{start\ year}+n} O_3^{\mathrm{month}_x,\mathrm{year}_y},$$

the ozone mean for each month of the year averaging over n year from start year to start year $+\,n$. We use those anomalies for merging different datasets without worrying about possible biases or different starting and finishing dates.

SECTION B: CROSS-COMPARISON BETWEEN GROUND-BASED AND SATELLITE DATASETS

We use comparisons with two different satellite datasets, IASI-CDR and MEGRIDOP, to evaluate the quality of all the ground-based time-series described above and to validate the long-term stability of ozone satellites data sets (presence or not of significant drifts in %/decade) for the whole Arctic zonal mean, both in the total column and for each partial column defined in section A.

The Infrared Atmospheric Sounding Interferometer (IASI) aboard the Metop satellites provides twice-daily global infrared measurements, from which ozone profiles are retrieved using the FORLI optimal-estimation algorithm (Hurtmans et al. 2012). A homogeneous ozone Climate Data Record (CDR) has recently been produced by EUMETSAT on behalf of AC SAF (AC SAF, 2025) using consistent IASI/Metop-A and -B Level 1 radiances (EUMETSAT, 2018) and Level 2 temperature and humidity profiles (EUMETSAT, 2022). The CDR, available until December 2023, can be extended with the near-real-time (NRT) dataset because both rely on the same retrieval version (FORLI v20151001). In the following, this combined dataset is referred to as IASI-CDR. The IASI-CDR O_3 product has been validated by Boynard et al. in (Boynard et al. 2025), who reported small total ozone biases ($< 1-2\%$), tropospheric differences of $10-12\%$, and long-term drifts below 3% per decade. It accurately captures seasonal and interannual variability and highlights a decrease in tropospheric ozone, notably in the tropics and Europe. In this study, IASI O_3 total columns are obtained from the AERIS Level-3 monthly IASI-A and -B products (Clerbaux and Coheur 2025a, 2025b), while partial columns are derived from monthly mean IASI-AB gridded profiles computed from the AERIS Level-2 daily products as in (Keppens 2025). Both datasets cover 2008–2024 and we use daytime observations only.

The MErged GRIdded Dataset of Ozone Profiles (MEGRIDOP) (Sofieva et al. 2021) was generated using data from six limb and occultation satellite instruments (OSIRIS, GOMOS, MIPAS, SCIAMACHY, Aura MLS, OMPS-LP SNPP). We use the Level-3 gridded monthly time-series from 2001 until 2024, which has a $10°\mathrm{lat} \times 20°\mathrm{lon}$ horizontal resolution and a vertical coverage from $10-50$ km.

Our first aim is to compare satellite and ground-based time-series to diagnose potential problems related to the calculation of trends from those time-series. Therefore, we do not time-collocate satellites and ground-based measurements but instead we compute drifts by comparing monthly deseasonalized relative anomalies, that will later be used for trends computations. The time-series of satellites are spatially collocated within their respective precision grid with the ground-based instruments locations recalled in Table 1. To compare satellite and ground-based time-series, we define the difference of anomalies in percentage:

$$\mathrm{diff}^{i}_{\mathrm{sat-GB}} = \left(\mathrm{anom}^{i}_{\mathrm{sat}} - \mathrm{anom}^{i}_{\mathrm{GB}}\right) \cdot 100\%, \quad (3)$$

from which we obtain the relative bias and the scaled mean absolute deviation (MAD_s) between the two time-series (scaling with 1.4826 gives an equivalence to the 2σ of Gaussian statistics):

$$bias = \mathrm{median}\left(\mathrm{diff}^{i}_{\mathrm{sat-GB}}\right), \quad (4)$$

$$MAD_s = 1.4826 \cdot \mathrm{median}\left(\left|\mathrm{diff}^{i}_{\mathrm{sat-GB}} - \mathrm{bias}\right|\right), \quad (5)$$

We then apply a robust linear regression (Theil-Sen, (Sen 1968)) on the difference $\mathrm{diff}^{i}_{\mathrm{sat-GB}}$ to obtain the trend of this difference, i.e., the drift and its associated error, as shown in Figure 2 for the Vindeln Brewer against IASI ozone total columns.

The drift is estimated as the median of the slopes of all lines connecting all possible pairs of points. The confidence interval for the drift estimate is given by the interval containing the middle 95% (to obtain an estimate of the 2-σ error) of those slopes. The drift error is then the maximum between the difference of the upper bound of the confidence interval with the median and the lower bound of the confidence interval with the median.

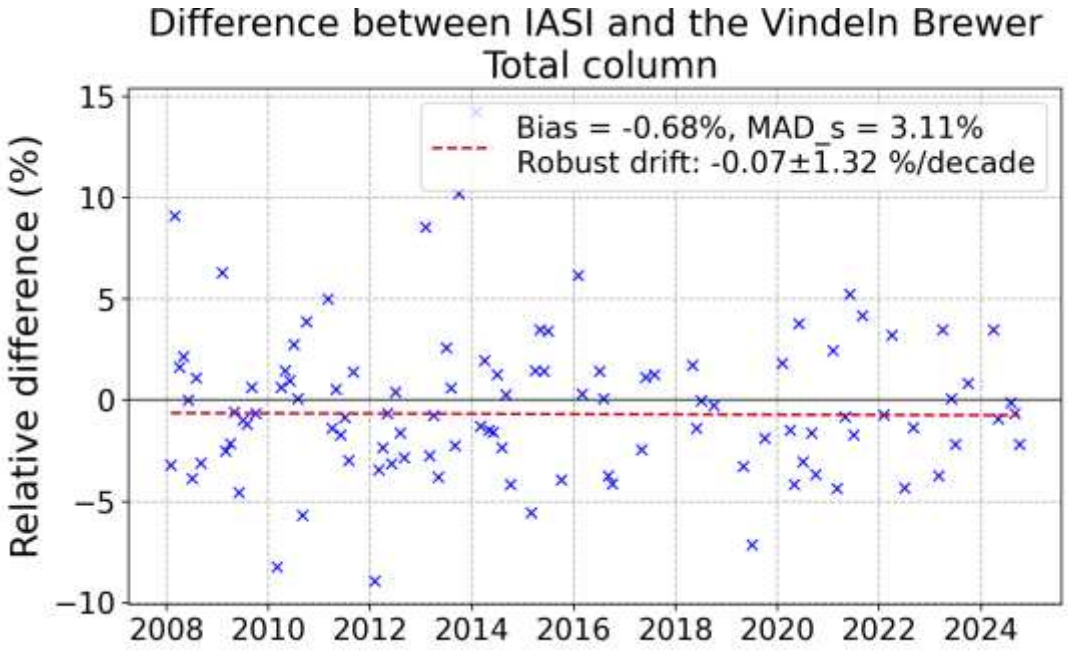

Figure 2: Difference of relative anomalies in percent $\mathrm{diff}^{i}_{\mathrm{sat-GB}}$ between the Vindeln Brewer total column and the IASI-A+B total column in Vindeln with associated bias, MADs and drift with 2σ-error. The presence of several strong outliers requires the use of a robust regression method, here the Theil-Sen method.

SECTION C: REPRESENTATIVENESS STUDY

An important drawback of ground-based measurements of atmospheric species compared to satellites measurements is the limited spatial coverage of the data. Despite the use of various instrument types, we only consider sixteen different sites where ozone is measured over a sufficiently long time-period, spanning a region from 60 to $90°N$, equivalent to a surface area of 34 million kilometers square. On the other hand, the long-term trends we are trying to observe are known to be small and drowned out by the large natural variability of ozone in the Arctic. To reduce uncertainties and obtain statistically significant trends, it is advantageous to combine several datasets which are geographically close. But what is a good criterion to combine datasets together? And what will be the spatial extent that the trends of these combined datasets really represent? To answer these questions, we perform a representativeness study like that of (Weatherhead et al. 2017). We also conducted a similar representativeness study based on CAMS data for tropospheric ozone but globally in Van Malderen, et al. (2025). We use the CAMS global reanalysis (EAC4) monthly averaged fields (Inness et al. 2019) of ozone to calculate the correlation of ozone time series between the locations of each of our ground-based stations. This enables us to define groups of stations that are highly correlated, and for which we create merged ground-based datasets used in trend calculation. We further define the representativeness of each of those groups of stations by calculating the correlations of ozone time-series at those stations with ozone time-series in the rest of the Arctic. The CAMS dataset is a gridded dataset with a global coverage and a spatial resolution of $0.75° \times 0.75°$, with a temporal coverage from $2003 - 2024$. We use the ozone total column and the vertically gridded ozone profile given in 25 pressure levels that we sum in four partial columns as shown in Table 3.

Correlations are calculated based on monthly deseasonalized absolute anomaly (Eq. 2) time-series (correlations of ozone column time-series mostly reflect the seasonal cycle of ozone which accounts for most of ozone annual variability). Therefore, the correlations represent the similarity in ozone variability independent of the seasonal cycle. For each ground-based station, we thus compute the Pearson correlation coefficient $r_{x,y}$ between the CAMS monthly anomaly at the grid-cell where that site is located, x, and the CAMS monthly anomalies for each of all the other cells, y, located in Arctic (60-90°N):

$$r_{x,y} = \frac{\sum_{i=1}^{n}(x_i - \bar{x})(y_i - \bar{y})}{\sqrt{\sum_{i=1}^{n}(x_i - \bar{x})^2}\sqrt{\sum_{i=1}^{n}(y_i - \bar{y})^2}}\ ; \qquad (6)$$

where x_i, $i \in (1, \ldots, n)$ is the time series of ozone at the site location x, $\bar{x}$ is the mean of that time series, and similarly for y at all other locations of the grid. We check that our results are physically sensible by analysing the scatterplots of absolute anomalies between each ground-based station location.

SECTION D: CALCULATING REGIONAL TRENDS

MERGED DATASETS

We calculate trends based on merged datasets obtained from weighted means of ozone anomalies (Eq. 1) time series. Starting from N different anomalies datasets, anom_α, their weighted merging is calculated as:

$$\text{anom}_{\omega-\text{m}} = \frac{\sum_{\alpha=1}^{N} \omega_\alpha \ \text{anom}_\alpha}{\sum_{\alpha=1}^{N} \omega_\alpha}. \qquad (7)$$

The weight used for merging is the inverse square of the anomalies errors, $\omega_\alpha = 1/(\Delta\text{anom}_\alpha)^2$. But since systematic errors are affecting all values of the time-series in the same way, we ignore them when considering anomalies and we only propagate random uncertainties (considered as statistically independent) into the daily and monthly means of ozone columns and the monthly ozone anomalies. Starting from the individual measurement's random uncertainties of the ozone timeseries, $\Delta O_3^{individual}$, we calculate the uncertainties on the daily means ΔO_3^{day}, with N_{day} the number of measurements in that specific day, and then we further propagate the random error to the monthly mean to obtain ΔO_3^{month}, with N_{month} the number of days of measurement within that month:

$$\Delta O_3^{\mu=\{\text{day, month}\}} = \frac{1}{N_\mu}\sqrt{\sum_{\beta=1}^{N_{\mu\alpha}}\left(\Delta O_3^{\beta}\right)^2} \quad with\ \beta = \{individual, day\}\ respectively.$$

Finally, the error on the monthly relative anomalies (Eq. 1) is given by:

$$\Delta\text{anom}^{\text{month}_x,\text{year}_y} = \frac{1}{O_3^{\text{month}_x}}\sqrt{\left(\Delta O_3^{\text{month}_x,\text{year}_y}\right)^2 + \left(O_3^{\text{month}_x,\text{year}_y}\cdot \Delta O_3^{\text{month}_x}/O_3^{\text{month}_x}\right)^2}.$$

The random error on relative anomalies has the same dimension as $(\Delta O_3)/O_3$. This value is given for each instrument and column in Table 4 in percentage.

Instrument	Column	Δanom
Brewer	TCO	0.449 %
Dobson	TCO	1.067 %
FTIR	TCO	0.413 %
FTIR	0-8km	1.481 %
Sondes	0-8km	1.714 %
FTIR	8-17km	0.986 %
Sondes	8-17km	0.545 %
FTIR	17-26km	0.908 %
Sondes	17-26km	0.316 %
FTIR	26-48km	1.179 %

Table 4: Averaged random error for anomalies for each instrument and each ozone column.

REGRESSION MODEL AND PROXIES

Stratospheric ozone trends are expected to be small (within a few %/decade) while the natural ozone variability is especially high in the Arctic (Brasseur and Solomon, 2005; Langematz et al., 2018). This means a simple linear regression is not sufficient to detect long-term trends with good uncertainties. In this work, trends are calculated with a multiple-linear regression (MLR) using nine different proxies summarized in Table 5. These proxies account for the natural variability of ozone, thus reducing trends uncertainties. The proxies are similar to those used by Vigouroux et al. (2015), except that for the processes included in the LOTUS MLR model (Petropavlovskikh et al., 2019), namely Solar cycle, QBO, and ENSO, we used the LOTUS prescribed data sets made publicly available within the OREGANO project (https://www.iup.uni-bremen.de/OREGANO/proxydata/). For Arctic Oscillation (AO) and Brewer-Dobson Circulation (BDC) proxies, we also use data sets provided within OREGANO, for which

the accumulation during Winter months has been considered (Weber et al., 2022). The Volume of Polar Stratospheric Clouds (VPSC) have been calculated as the volume of air between the 370 K and 550 K potential temperature levels, where the temperature is below the formation temperature of ICE or NAT clouds, using ERA5 temperature. We assumed a formation temperature of 185 K for ICE clouds and 194 K for NAT clouds (Rex et al., 2004). We also consider the accumulation during Winter following (Brunner et al., 2006). The local proxies (tropopause pressure (TP), equivalent latitude (EL) and stratospheric temperature (T)) have been taken from ERA5 reanalysis at the location of each station. Then for each region, we use as final TP, EL, and T proxies the mean of these local proxies at the sites included in a single region (4). The EL and T proxies are calculated for the three stratospheric columns, leading to six proxy time series (called LS, MS, and US for the lower, middle and upper stratospheric columns, see Table 3). For each partial column, the mean of the EL (T) values in the corresponding ERA5 vertical layers is used. From all these proxies, only the local stratospheric temperature proxy is new compared to (Vigouroux et al., 2015).

Since we use monthly anomalies (Eq.1) for the determination of the trend, all the proxies are also deseasonalized, and we model the monthly anomalies time series $a(t)$ as:

$$a(t) = A_1 + A_2 \cdot t + \sum_{n=3}^{m} A_n \cdot X_n(t) + \varepsilon(t),$$

where $X_n(t)$ are the explanatory variables (i.e., proxies) with A_n their regression coefficient and A_2 is the estimated trend. We only consider the trend after 2000 so the turnaround should have already happened before the start of the time-series and only one linear term is sufficient to describe the actual trend. The trend error is given at the 2σ level and multiplied by a specific factor to account for autocorrelation (see (Santer et al. 2008), alternative to the Cochrane-Orcutt method). Finally, $\varepsilon(t)$ is the residual (difference between the regressed model and the real data).

	Proxy used
Solar cycle	Bremen composite Mg II index
QBO	Principal components zonal mean wind 6°S – 6°N (ERA5)
ENSO	Multivariate ENSO Index (MEI)
AO	Arctic Oscillation Index
BDC	Eliassen-Palm (EP) Flux at 100hPa
VPSC	Volume of Polar Stratospheric Clouds (not used in the upper stratosphere)
TP	Tropopause Pressure at each station location (ERA5)
EL	For each of the three stratospheric columns: Local Equivalent Latitude averaged over the corresponding column (ERA5)
T	For each of the three stratospheric columns: Local Temperature averaged over the corresponding column (ERA5)

Table 5: The nine proxies used in the MLR for attribution of ozone variability in ozone trends.

For each trend calculated, a stepwise procedure determines the relevant proxies used in the regression (Mäder et al. 2007), which can then differ by region and partial column. Each of those relevant proxies adds an individual contribution C_{frac} to the coefficient of determination $R^2 = \sum C_{\text{frac}}$. This individual contribution is calculated as the product of the standardized regression coefficient of the proxy with the correlation coefficient between the proxy and the observed dataset. The coefficient of determination then represents a statistical measure of the goodness of fit, i.e., how well the regressed model matches the datasets variability.

Several proxies, such as the temperature and equivalent latitude proxies, are often correlated (up to $|r| = 0.8$) but thanks to the stepwise regression method, both can be included without overfitting. In cases where the stepwise procedure still selects two proxies with high correlation, we explicitly verify that their combined use positively improves the fitting of the model to the datasets (i.e., leads to a higher coefficient R^2 without increasing the uncertainty on the trends). The median value of the absolute correlations between proxies is of about $r = 0.15$.

Finally, some of the proxies used in the MLR can exhibit a trend. Whether or not these proxies' trends should be part of the ozone trend depends on what we are trying to measure. The VPSC for instance possesses a positive trend over the last two decades (von der Gathen et al. 2021; Pazmiño et al. 2023) due to climate forcing, which can be related to an increase of ozone depletion in the lower and mid stratosphere. By including this proxy, together with its trend, in our MLR, we are effectively computing the ozone trend that is not due to this VPSC-related depletion. In the context of this study, this choice is justified by our aim in assessing the impact of the Montreal Protocol and its amendments, i.e., detecting the stratospheric ozone recovery associated with the diminution of ODS in the stratosphere. To assess the impact that these proxies' trends may have on the effective ozone levels and to understand the dependency of our conclusions on each of them, we perform a sensitivity analysis by detrending each proxy individually. For each, we compare trends calculated using the original versus the detrended proxy, and we report on significant differences.

4. SCIENTIFIC RESULTS AND RECOMMENDATIONS

RESULT 1: SELECT THE BEST QUALITY GROUND-BASED TIME SERIES IN ARCTIC

NEW FTIR RETRIEVAL IN SODANKYLÄ

As explained in the FTIR dataset description above, the FTIR instrument in Sodankylä is part of the TCCON (Total Carbon Column Observing Network) rather than NDACC and measures in a different spectral range. Based on the retrieval strategy from Zhou et al. (2020), we have performed the retrieval of ozone in the $3040\ cm^{-1}$ spectral region with a vertical resolution of about 2.5 DOFS. We have generated a completely new ozone dataset for FTIR at Sodankylä providing a stratospheric ozone column between 10-50 km, as well as information about the lower, mid and upper stratosphere (see the DOFS repartition in Table 1). An example of the spectral window transmission signal and of the retrieved profile is shown in Figure 3.

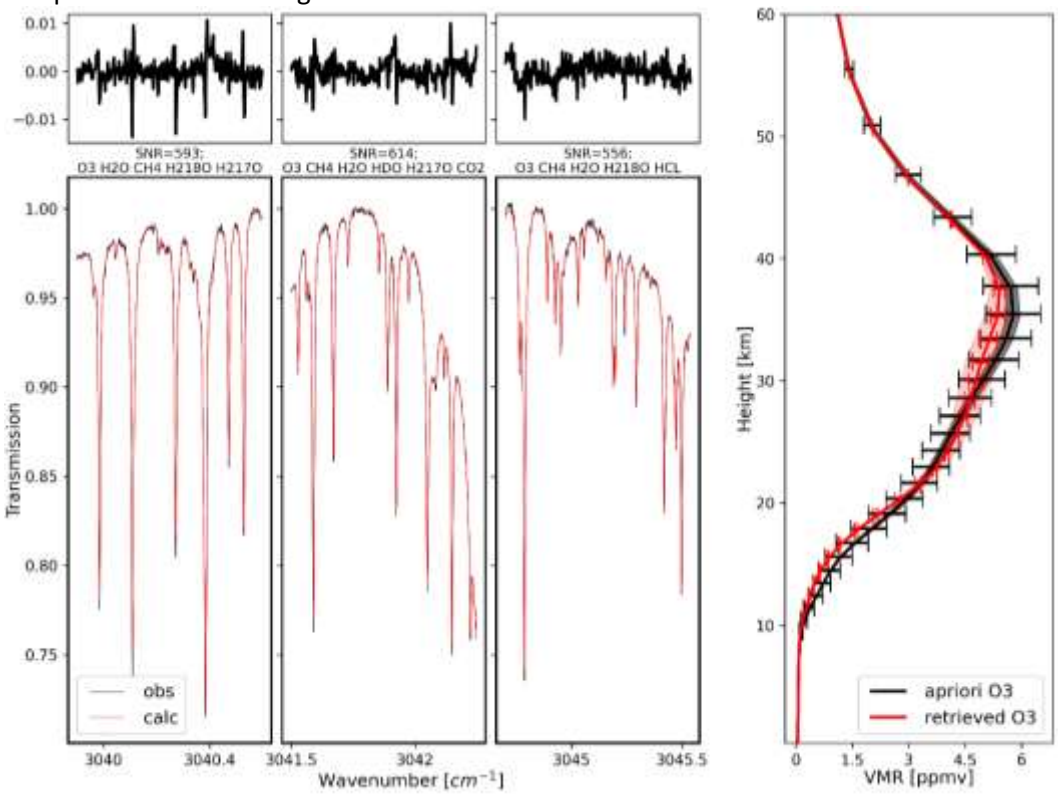

Figure 3: Example of the Sodankylä TCCON FTIR signal in the spectral windows around $3040\ cm^{-1}$ used for ozone retrieval and the corresponding ozone profile retrieved in volume mass ratio (vmr).

EVALUATION OF GROUND-BASED DATASETS USING SATELLITES

Because MEGRIDOP is based on Limb satellites that do not measure in the troposphere, ground-based measurements of the tropospheric column and the total column can only be compared to IASI-CDR (see Figure 4 for a visual representation of the vertical coverage of profile data sets versus the chosen partial column layers). Moreover, because MEGRIDOP only starts at 10 km, we consider an alternative lower stratospheric column from 10–17 km. This alternative lower stratospheric partial column can be easily computed and still retains enough DOFS for the FTIR (see Table 1). The reason why we

selected 8−17 km as our main lower stratosphere column is because we want to be able to compare total column trends to the sum of partial column trends (i.e. not missing the 8-10km layer).

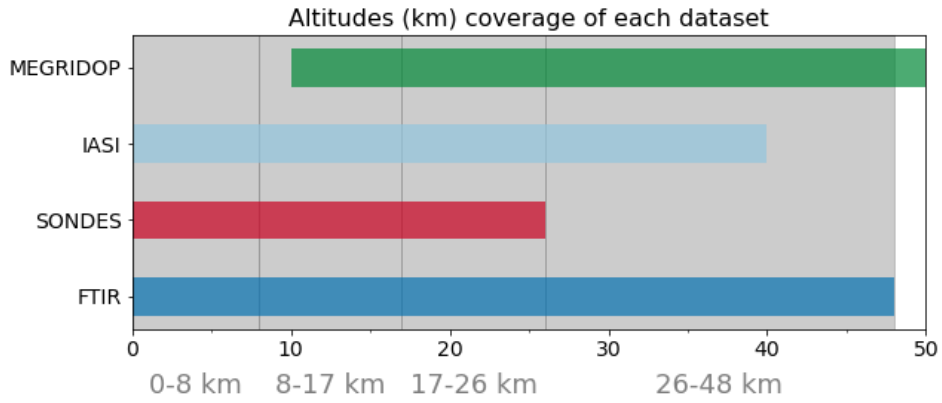

Figure 4: Vertical coverage of each profile data sets used in this study against our choice for partial columns altitude boundaries.

We do not identify any outliers in the total column ground-based time series. We find all drifts lay within $|1.6\%/decade|$ (see Figure 5 left). Only the drifts in Fairbanks and Alert are at the limit of 2σ significance, reaching respectively (-1.17 ± 1.06) and (-1.59 ± 1.41) $\%/decade$. Even though this might indicate potential issues around that time period (2007-2024), we do not exclude those timeseries from our trend analysis, as we will in fact consider the full 2000−2024 period and the drifts reported here are overall very small. Also, the overall IASI comparisons are mainly showing small negative drifts, suggesting that it is due to the satellite.

In the troposphere, see Figure 5 right, IASI-CDR exhibits a significant negative drift of at least $-6\%/decade$ with seven of the ground-based instruments. This points toward an overall negative drift of IASI-CDR in the troposphere that we will comment on in next section. IASI-CDR is more negatively drifted with the St-Petersburg FTIR (about $-14\%/decade$), but this dataset only starts in 2009. The Scoresbysund sonde however clearly stands out with a positive drift in IASI-CDR of $(+11.51 \pm 3.58)\%/decade$, significant beyond the 5σ level, signalling a problem with this time series.

Turning to the stratospheric column drifts of both IASI (on the 2007-2024 period) and MEGRIDOP (on the 2001−2024 period) with respect to all individual ground-based instruments in Figure 6, we find that the Scoresbysund sonde also stands as an outlier in the lower and mid-stratosphere for both satellites. The drift is associated with a negative offset in the Scoresbysund ozone concentrations at most altitude levels in the ozonesonde time series since 2016 with respect to the previous years. Indeed, we have verified that the Scoresbysund's sonde dataset does not show any significant drift with respect to MEGRIDOP over the prior 2001−2015 period, where we found a drift of about $4\%/decade$ in the 10−17 km layer and of about $2\%/decade$ in the 17−26 km layer, both non-significant. This drop in 2016 coincides with a change of ozonesonde type, ozonesonde pump battery type and radiosonde type, leading resp. to a 3−4% bias in the ozone concentrations, lower pump temperatures (around −10K), and a possible offset in the atmospheric pressure measurements (switch from pressure sensor to GPS height derived pressure measurements). The homogenization of the Scoresbysund time series at the HEGIFTOM repository only corrects for the first effect. The other two issues might be responsible for a drop in the ozone concentrations, e.g. too low pump temperatures might point to freezing solutions and too low signal readings and a shift of the entire profile with +1.5 hPa at mid-stratospheric pressure levels. Unfortunately, these issues need further investigation and adequate correction algorithms have not been developed yet, so we remove the Scoresbysund ozonesonde dataset from our study.

The Resolute sonde also appears as an outlier in MEGRIDOP's drifts for the lower and mid-stratosphere but not in IASI-CDR's drifts. By comparing the drifts on the same time period (2007−2024), the MEGRIDOP's drifts at Resolute disappear, see Figure 8. In fact, we see a progressive diminution of the drift that becomes non-significant starting from 2005. This is probably the signal of a jump in the sonde dataset possibly due to instrumentation changes. Recalibrations in the data sets to account for these various changes have already been performed in Resolute (see Tarasick et al., 2016) but additional jumps cannot be excluded. Despite these recalibrations, it was found in Figure 17 of Tarasick et al. (2016) and Figure 3 of Nilsen et al. (2024) that the Resolute sonde exhibits stronger significant negative trends in the lower stratosphere than other sondes in the Arctic (except for the Churchill sonde that lies below our 60◦N limit). To avoid effects of this potential jump, we consider the Resolute sonde dataset only starting from 2005.

In the upper stratosphere (26−48 km, Fig. 6), IASI-CDR possesses small negative drifts everywhere except at Kiruna, where it shows a singular significant positive drift above 3%/decade. The drift of MEGRIDOP in Kiruna doesn't particularly stand out on the 2001−2024 period, but if we restrict both satellites to the same 2007−2022 time period (Kiruna time series stops in 2022, see Table 2), we observe a similar pattern where all drifts are non-significant and within $3\%/decade$ except in Kiruna where they reach $(3.56 \pm 2.31)\%/decade$ for IASI-CDR and $(4.91 \pm 2.08)\%/decade$ for MEGRIDOP, see Figure 9. There are no records of possible issues with the Kiruna FTIR time series and visual scrutiny of its monthly mean and anomalies time series doesn't reveal obvious jumps. As the drift value with MEGRIDOP using the full time series (Fig. 6) is comparable to other FTIR stations (although significant at Kiruna), we retain Kiruna for our trend analysis on the full time period.

Finally, in the total stratospheric column (10−50 km, see Figure 7), IASI-CDR does not exhibit any significant drift except with Sodankylä FTIR. That time series is retrieved from a different spectral range than other NDACC FTIR products but there is no trace in previous studies of a potential drift due to this method of retrieval (Garcia et al., 2014; Zhou et al., 2020). It is also the only time series that starts in 2012 so the starting date for IASI-CDR comparison is different from all other data sets. Also, this station is not an outlier when compared to MEGRIDOP (10−50 km, see Figure 7).

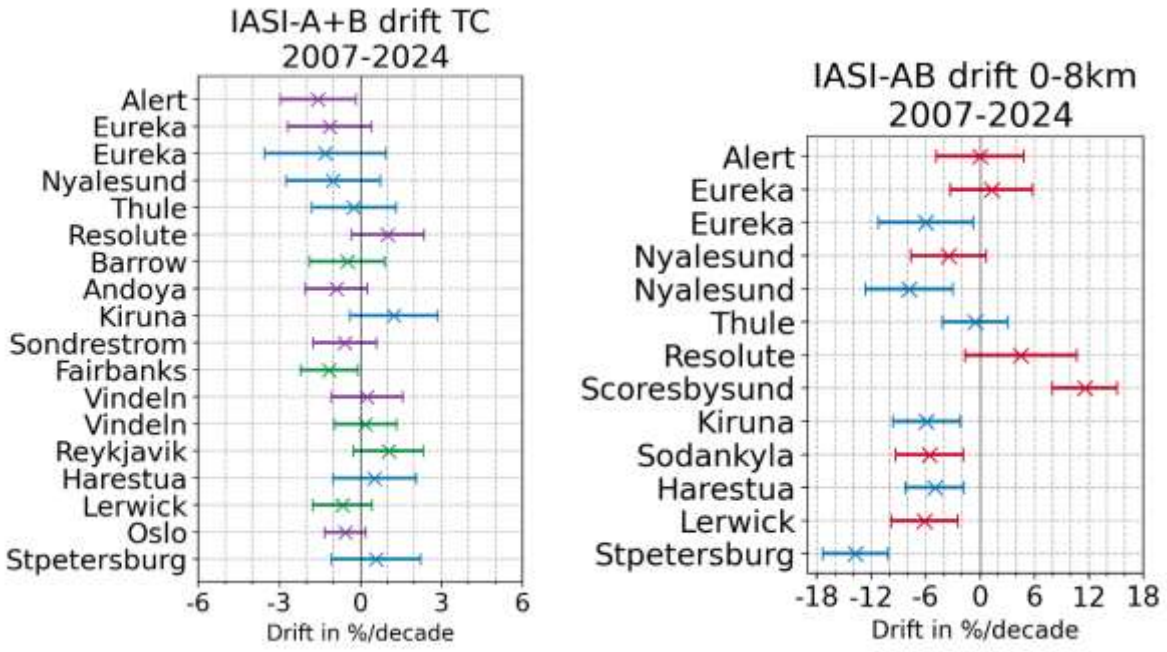

Figure 5: Robust drift of IASI-CDR on the full 2007−2024 period for the total column (left) and tropospheric column (right) with respect to all individual FTIR, ozonesondes, Brewer and Dobson instruments in percent per decade, with a 2σ-error. Instruments are ordered by decreasing latitude from top to bottom, and trends are color-coded depending on the instrument (purple: Brewer, green: Dobson, blue: FTIR, red: ozonesondes).

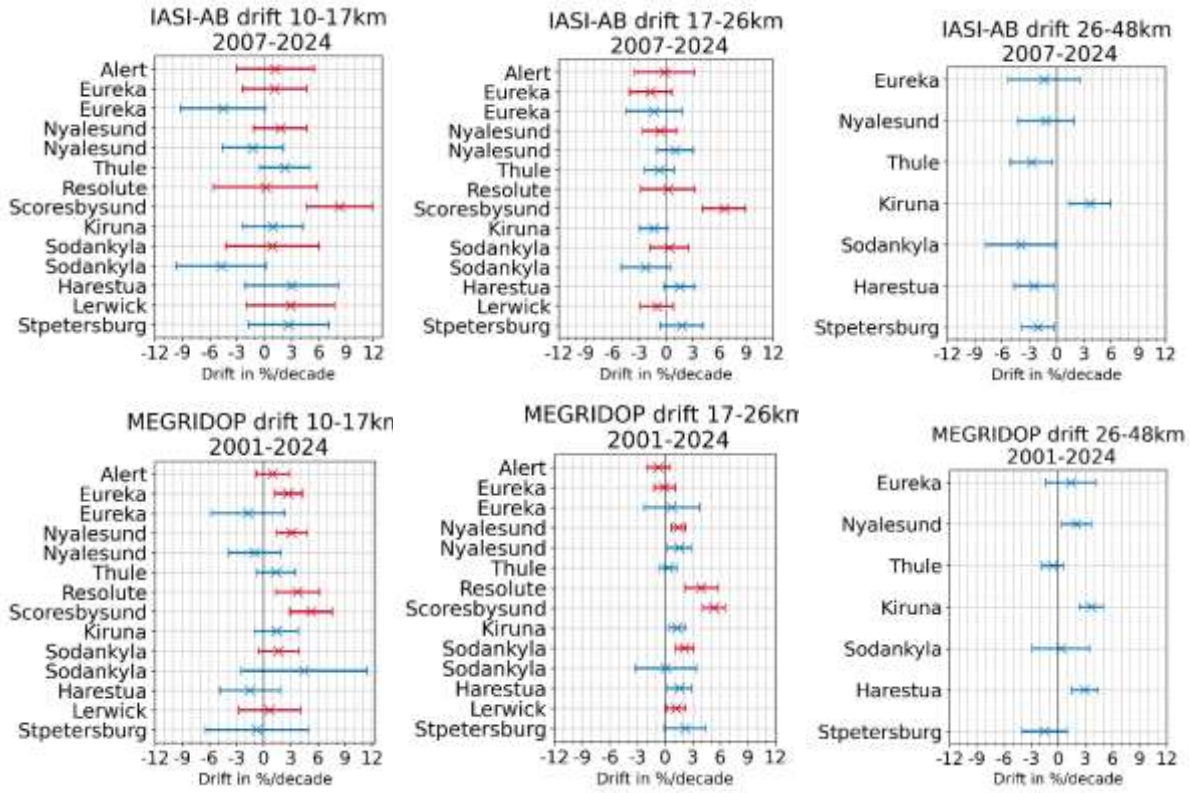

Figure 6: Robust drifts of IASI-CDR (2007−2024) and MEGRIDOP (2001−2024) with respect to ground-based measurements in the stratosphere in %/decade with 2σ errors. The time periods given in the title of each figure refers to the satellite time periods, though some ground-based time series are more limited, see Table 2.

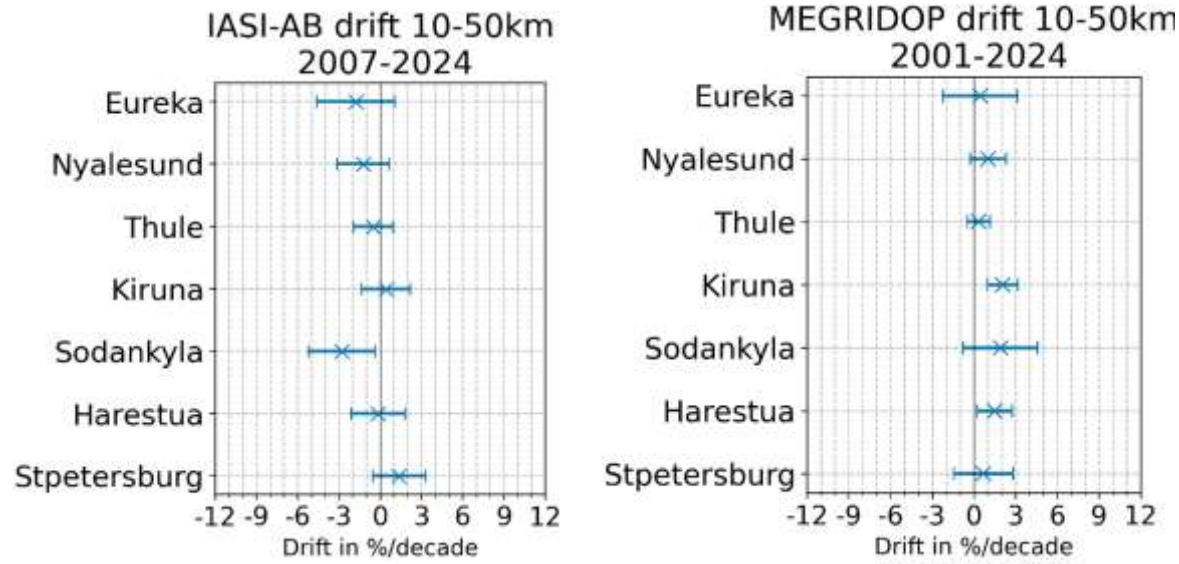

Figure 7: Robust drift of IASI-CDR and MEGRIDOP with respect to ground-based measurements for the total stratospheric column (10-50 km).

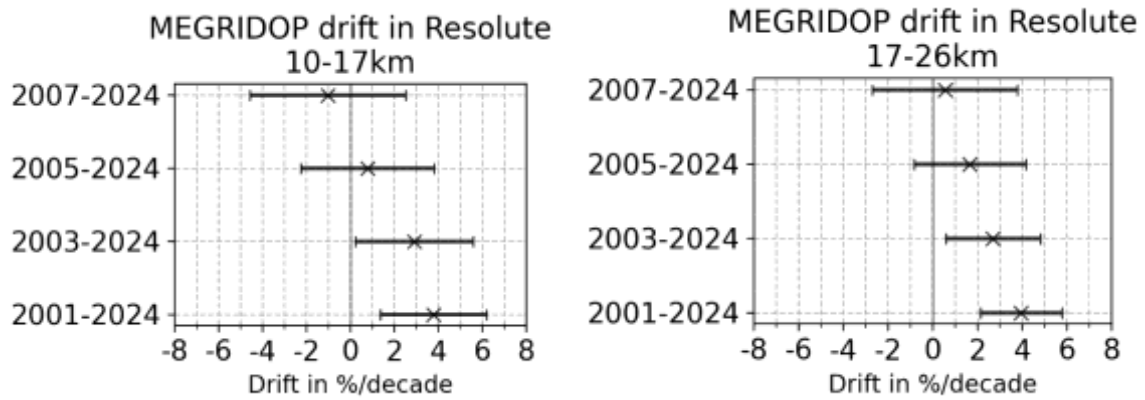

Figure 8: Variation of the drift of MEGRIDOP with respect to the Resolute sonde in lower and mid-stratosphere depending on the starting date of comparison.

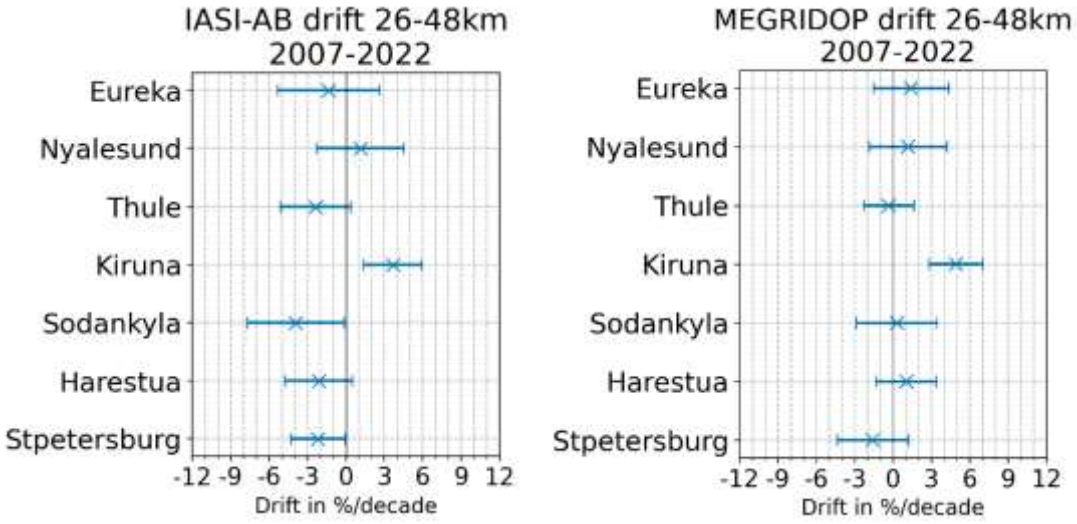

Figure 9: Drifts of MEGRIDOP and IASI-CDR with respect to the FTIR data sets in the upper stratosphere when restricting to a common period of 2007 to 2022.

DRIFTS OF SATELLITE DATASETS USING GROUND-BASED MEASUREMENTS

Putting aside problematic ground-based time series, we average all remaining datasets by a weighted mean (weights are given by the inverse squared uncertainties) and compare this average with the mean of satellites time series at the site locations. The resulting zonal band drifts of IASI-CDR and MEGRIDOP are presented in Figure 10.

The zonal mean drift of IASI-CDR total column is of $(-0.63 \pm 1.01)\%/decade$. This is a very small uncertainty, and it shows that the IASI-CDR Level 3 AERIS total column product is not drifted over its full time series.

In the troposphere we find that IASI-CDR has a negative significant drift of $(-3.47 \pm 2.35)\%/decade$. This can be explained by the sensitivity drop of IASI-CDR at high latitudes, especially in the troposphere. By computing the trace of the averaging kernels of IASI-CDR troposphere profiles at our 16 ground-based stations locations, we find it contains on average about 0.4 DOFS (see also Boynard et al. (2025)). A more precise determination of the IASI-CDR tropospheric drift would require smoothing out the ground-based measurements to the IASI-CDR sensitivity prior to comparison.

IASI-CDR doesn't show any significant drift in the lower, middle and total stratosphere. In the lower stratosphere the individual drifts are all within $|5\%/decade|$ (with a zonal mean drift within

$|3\%/decade|$), and in the middle and total stratosphere individual drifts lay within $|3\%/decade|$ (with a zonal mean drift within $|1.5\%/decade|$ and $|1\%/decade|$ respectively).
In the upper stratosphere, despite a negative significant drift at four individual stations, the zonal band drift of IASI-CDR is not significant and only about $1\%/decade$. Even if we exclude Kiruna (which is driving the mean to more positive values), that drift stays non-significant and reaches $(-1.42 \pm 1.62)\%/decade$.
MEGRIDOP is positively drifted with respect to the zonal mean of all ground-based instruments in the lower and upper stratosphere with drifts of $(2.76 \pm 1.48)\%/decade$ and $(1.97 \pm 0.97)\%/decade$ respectively. The smallness of these uncertainties is however remarkable, especially when considering the high variability of individual drifts in the lower stratosphere for instance.
In the mid-stratosphere, the zonal band drift of MEGRIDOP is smaller than $|1\%/decade|$ while all individual drifts lay within $|3\%/decade|$.
Finally, in the total stratospheric column, MEGRIDOP's zonal band drift lies at the limit of significance: $(0.87 \pm 0.82)\%/decade$. All individual drifts are also within $|3\%/decade|$. The smallness of the uncertainty is here also remarkable but is expected to be smaller in MEGRIDOP than for IASI-CDR since the time period of comparison is more extended.

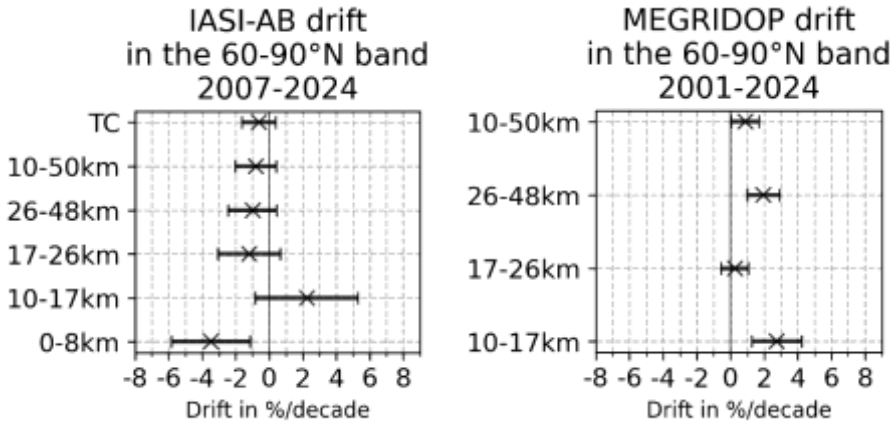

Figure 10: Drifts of satellites with respect to the weighted means of all ground-based instruments in each column. Problematic ground-based instruments (Scoresbysund, Resolute before 2005) are not included in the means.

RESULT 2: REPRESENTATIVE REGIONS

For each ground-based station, for the total column and the four partial columns of ozone, we obtain correlation maps such as in Figure 11 for the Eureka station. We consider each column separately because they all entail different sets of ground-based instruments (see Table 3) but also because the atmospheric dynamics and ozone chemistry vary with altitude, impacting the size of correlated regions in each layer.

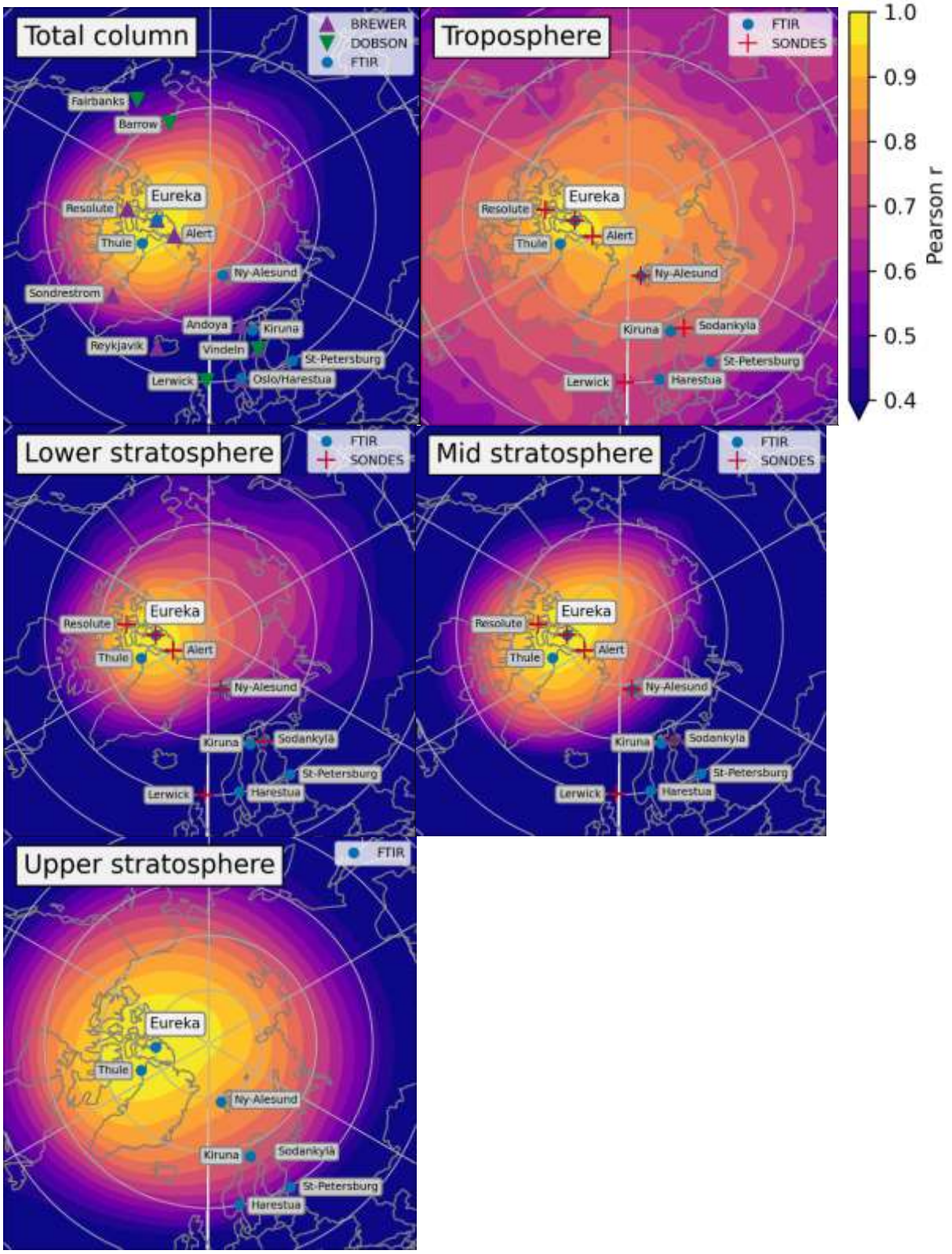

Figure 11: Correlation of CAMS deseasonalized anomalies at the location of the Eureka station with anomalies in the rest of the Arctic. Stations where a ground-based instrument is used in the corresponding partial column are indicated.

In the lower and mid-stratosphere (8-26 km), we find that regions with correlated ozone anomalies are smaller in extent than in the upper stratosphere, above 26 km. This is expected since photochemistry drives ozone variability in the upper stratosphere, while in the lower and mid-

stratosphere, dynamical activity dominates variability (Brasseur and Solomon, 2005). In the troposphere, very highly correlated regions ($r > 0.95$) are small like in the lower stratosphere, but correlated regions with $r \in [0.6,0.9]$ are very spread out. This is consistent with the fact that photochemical processes dominate ozone variability in the troposphere (Cooper et al., 2014) and that emissions of ozone precursors are low and relatively homogeneous across the 70º-90ºN region.
From the CAMS correlation maps, we define groups of stations such that within one group, the CAMS correlation of each member station with each other member stations must be higher than $r > 0.8$ (in Weatherhead et al. (2017), correlations of $r > 0.7$ are deemed "well correlated", while $r > 0.9$ are "strongly correlated"). The resulting regional groups are presented in Table 6. Some stations stand on their own and do not correlate well with any other stations. We consider them in our trend study only if their time series spans most of the 2000−2024 time period. For instance, Reykjavik and Sondrestrom in the total column are considered for trends, while St-Petersburg in the lower stratosphere and total column is not. Having defined the groups of stations whose time series will be combined to obtain trends with reduced uncertainties, we now determine the spatial regions for which these trends will be representative. A grid-cell on the map is part of a group's region if the correlation coefficients r of the grid-cell with each of the group's stations are all larger than 0.8. If a grid-cell is part of several regional groups, the prevalence goes to the group with the highest mean of correlations between each of its stations and the grid-cell. All regional groups for each atmospheric layer are depicted in Figure 12.

TCO	**Canada** FTIR: Eureka, Thule Brewer: Alert, Resolute, Eureka	**Ny-Ålesund** FTIR: Ny-Ålesund	**North Scandinavia** FTIR: Kiruna Brewer: Andoya, Vindeln Dobson: Vindeln	**North-West Europe** FTIR: Harestua Brewer: Oslo Dobson: Lerwick	**Alaska** Dobson: Barrow, Fairbanks	**Reykjavik** Dobson: Reykjavik	**Sondrestrom** Brewer: Sondrestrom
0-8 km	**North Pole** FTIR: Eureka, Thule, Ny-Ålesund Sondes: Alert, Resolute, Eureka, Ny-Ålesund		**Scandinavia** FTIR: Kiruna, Harestua, St-Petersburg Sondes: Sodankylä, Lerwick				
8-17km	**Canada** FTIR: Eureka, Thule Sondes: Alert, Resolute, Eureka	**Ny-Ålesund** FTIR & Sonde: Ny-Ålesund	**Lapland** FTIR: Kiruna, Sodankylä Sondes: Sodankylä	**North-West Europe** FTIR: Harestua Sondes: Lerwick			
17-26 km	**Canada** FTIR: Eureka, Thule Sondes: Alert, Resolute, Eureka	**Ny-Ålesund** FTIR & Sonde: Ny-Ålesund	**North-East Europe** FTIR: Kiruna, Sodankylä, St-Petersburg Sondes: Sodankylä	**North-West Europe** FTIR: Harestua Sondes: Lerwick			
26-48 km	**North Pole** FTIR: Eureka, Thule, Ny-Ålesund		**Scandinavia** FTIR: Kiruna, Sodankylä, St-Petersburg, Harestua				

Table 6: For each atmospheric layer, this table lists all data sets (classified by instrument) comprised in each of the groups we determined using the representativeness study and which are pictured on the maps in Figure 12. Within a group, all station locations correlate with $r > 0.8$. Across layers, we have aligned groups corresponding to similar regions to represent how we can later sum partial column trends and compare with total column trends. For instance, the Canada total column trend will be compared to the sum of the North Pole tropospheric trend, the Canada lower and mid stratospheric trends and the North Pole upper stratospheric trend.

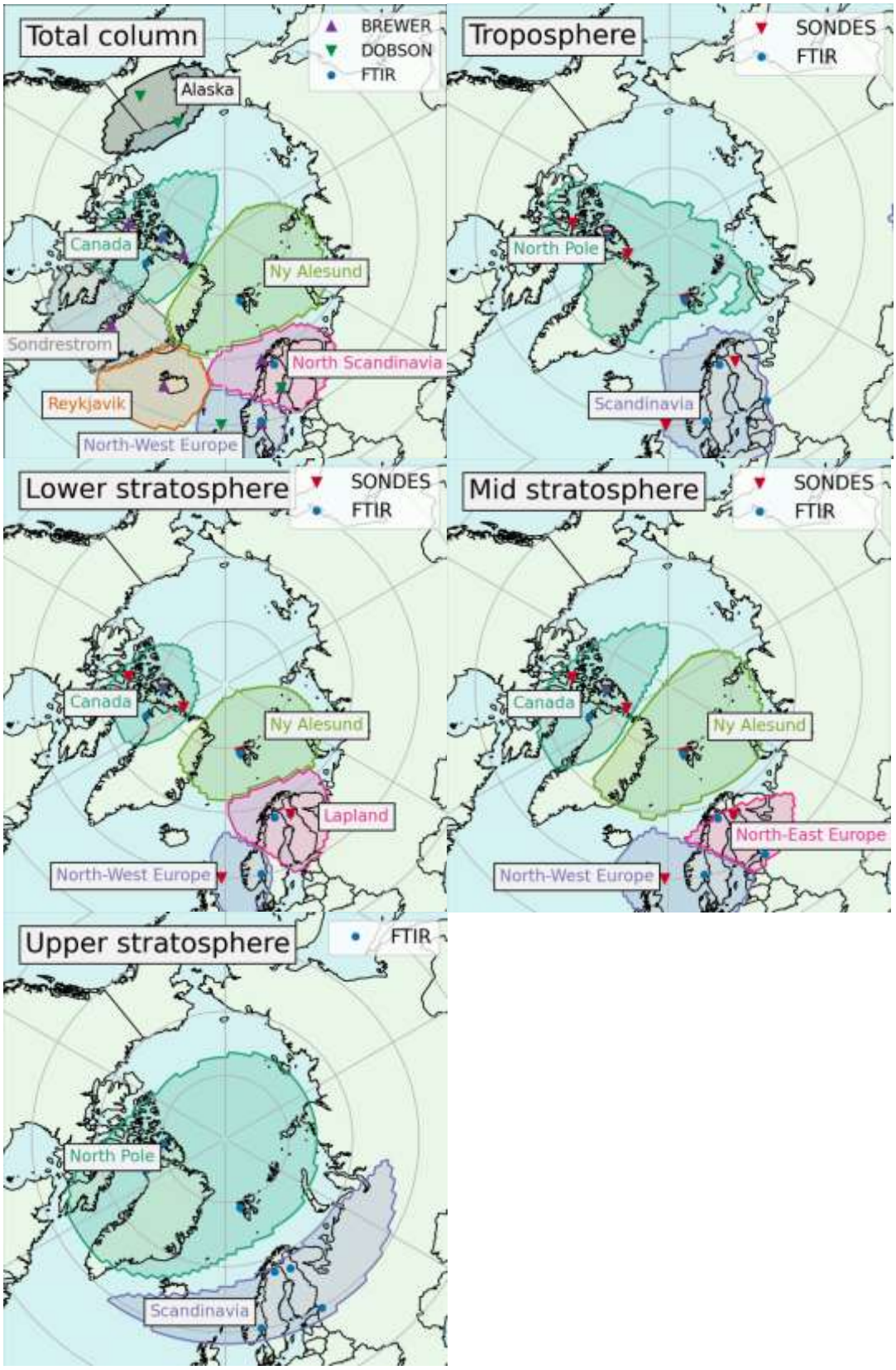

Figure 12: Regional groups for the total column and each partial column, listed in Table 4. We don't consider the St-Petersburg station in the total column and the lower stratosphere because it stands on its own there but has a too short time series (2009−2024). In the upper stratosphere, Ny-Ålesund correlates equally well with Eureka and Thule as with Kiruna and Sodankylä. Since Kiruna and Sodankylä also correlate with Harestua and Lerwick, while the two latter do not correlate at all with Ny-Ålesund, we have chosen to include Ny-Ålesund with the Canadian sites.

RESULT 3: ANNUAL AND SEASONAL OZONE TRENDS IN THE ARCTIC

PROXIES ANALYSIS AND SENSITIVITY TEST ON DETRENDING

We analyse in detail the total coefficients of determination R^2 together with the individual contributions from each proxy for all partial columns, as depicted in the charts of Figure 13 for the annual trends of merged anomalies data sets.

First, we consider proxies correlations. The temperature and equivalent latitude proxies are often correlated (up to $|r| = 0.8$ for the T_{LS} and T_{MS} in the total column) but thanks to the stepwise regression method, both can be included without overfitting. In cases where the stepwise procedure still selects two proxies with high correlation, we explicitly verify that their combined use positively improves the fitting of the model to the data sets (i.e., leads to a higher coefficient R^2 without increasing the uncertainty on the trends). The median value of the absolute correlations between proxies is of about $|r| = 0.15$.

In all columns, the tropopause pressure (TP) doesn't contribute significantly to any of the merged regions but is relevant for the single-site regions, namely Ny-Ålesund, Reykjavik and Sondrestrom. The TP is largely influenced by the seasonal cycle, thus strongly correlates with monthly ozone means (Hoinka et al., 1996; Steinbrecht et al., 1998), but a correlation persists for deseasonalized anomalies (Coldewey-Egbers et al., 2022). The TP has sometimes been used as a proxy in single-site ozone trends (Vigouroux et al., 2015; Bernet et al., 2023). Because it reflects mainly local variability, in general it is not used when calculating satellite trends over zonal bands (Sofieva et al., 2021; Weber et al., 2022; Godin-Beekmann et al., 2022). The averaging of the TP time series over a region likely removes most of the correlations between ozone and TP at individual sites. However, a positive correlation between the ozone anomalies and the TP was found also for the North-Atlantic region in Coldewey-Egbers et al. (2022), so this feature may vary depending on location and region's size.

In the total column, we find that the variability is mostly explained by the lower and mid-stratospheric temperature (T_{LS} and T_{MS}) and by the VPSC. As in partial columns, the AO, BDC, QBO, Solar cycle and equivalent latitudes account for smaller parts of the variability. The overall R^2 values lay between $0.5 - 0.6$, except in Reykjavik where it reaches beyond 0.8.

When analysing contributing proxies to seasonal trends, we observe an overall homogeneity of proxies throughout regions, further strengthening the confidence in the results. The variability is in general best explained in Spring, with R^2 values about 0.7 for the total column, reasonably well explained in Winter and Summer, and much less explained in Autumn, especially for merged groups of several stations. This is an interesting result, as the Arctic ozone loss due to ODS is expected to be the most important in Spring.

Finally, we have performed a sensitivity analysis to the VPSC proxy by running the trend analysis without including this proxy. We find that part of the variability explained by the VPSC is taken up by other proxies in its absence, in majority the BDC. This strong correlation between VPSC and BDC is well-known: a weak BDC is linked to lower temperatures and stronger vortex, and those conditions lead to more formation of PSCs (Langematz et al., 2018). Both VPSC (Rex et al., 2004) and BDC proxy (Weber et al., 2011) are linked to the same dynamical phenomena and correlate strongly with polar chemical ozone loss. The QBOs, AO, TP, EL and T contributions also increase to a lesser degree. In general, about half of the variability previously explained by the VPSC is not covered up by other proxies, resulting in a coefficient of determination R^2 smaller by up to 0.3 in the lower and mid-stratosphere where the effect of VPSC is the strongest. Contrary to what was found in Bernet et al. (2023), we see that adding the VPSC proxy improves our model's fit in the total column.

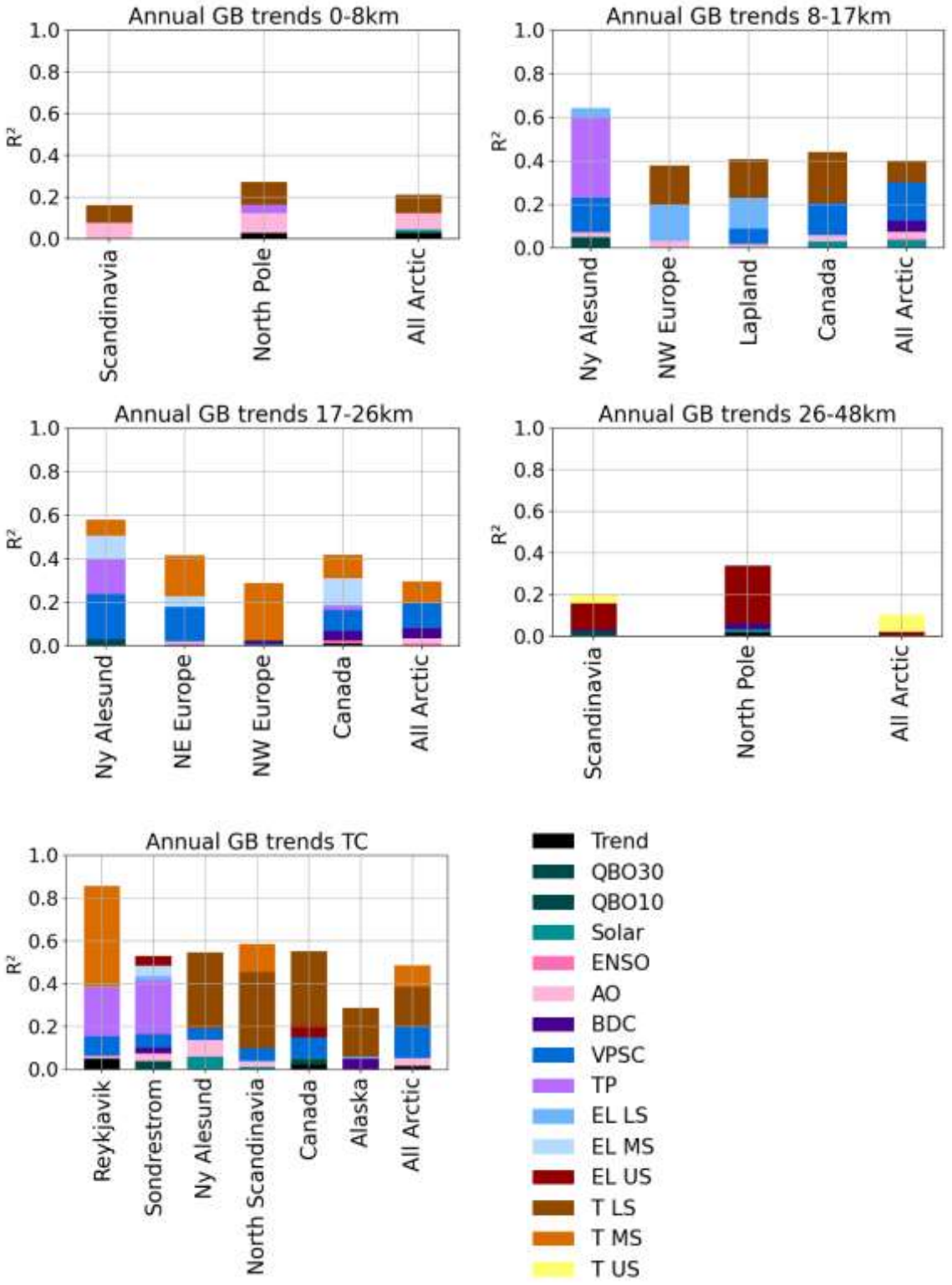

Figure 13: R^2 with individual contributions of proxies for all annual trends of ground-based instruments merged anomalies data sets for partial and total columns of ozone.

We start by analysing the total column trends results depicted in Figure 14. For this and all other columns, exact numbers with the associated 2σ uncertainties, given both in %/decade and in DU/decade, are provided in the Annexes. We have calculated annual trends which account for the full ozone anomalies time series, as well as seasonal trends divided in Winter (December-January-February), Spring (March-April-May), Summer (June-July-August) and Autumn (September-October-November). It is important to keep in mind that Winter (and sometimes Autumn) trends only consist of sondes profile in partial columns and of less precise measurements for Dobson and Brewer in the total column, especially at the highest latitudes where the polar night extends from October to February. We only calculate trends for time series with more than a certain number of data points (80 for annual trends and 25 for seasonal trends), so some Winter or Autumn trends in the total column and upper stratosphere, where only FTIR are present, are not calculated. Fewer data points in Winter also implies that the variability is always larger for that season. In the total column, trends are found to be overall positive. Except in Spring, there are some small negative trends but always non-significant. The trends in Canada, Reykjavik and Sondrestrom are always positive. The Lapland trend is negative only in Winter, the Alaska one only in Autumn and the Ny-Ålesund one only in Summer. Many positive trends are significant, especially in Spring, signalling the ozone recovery.

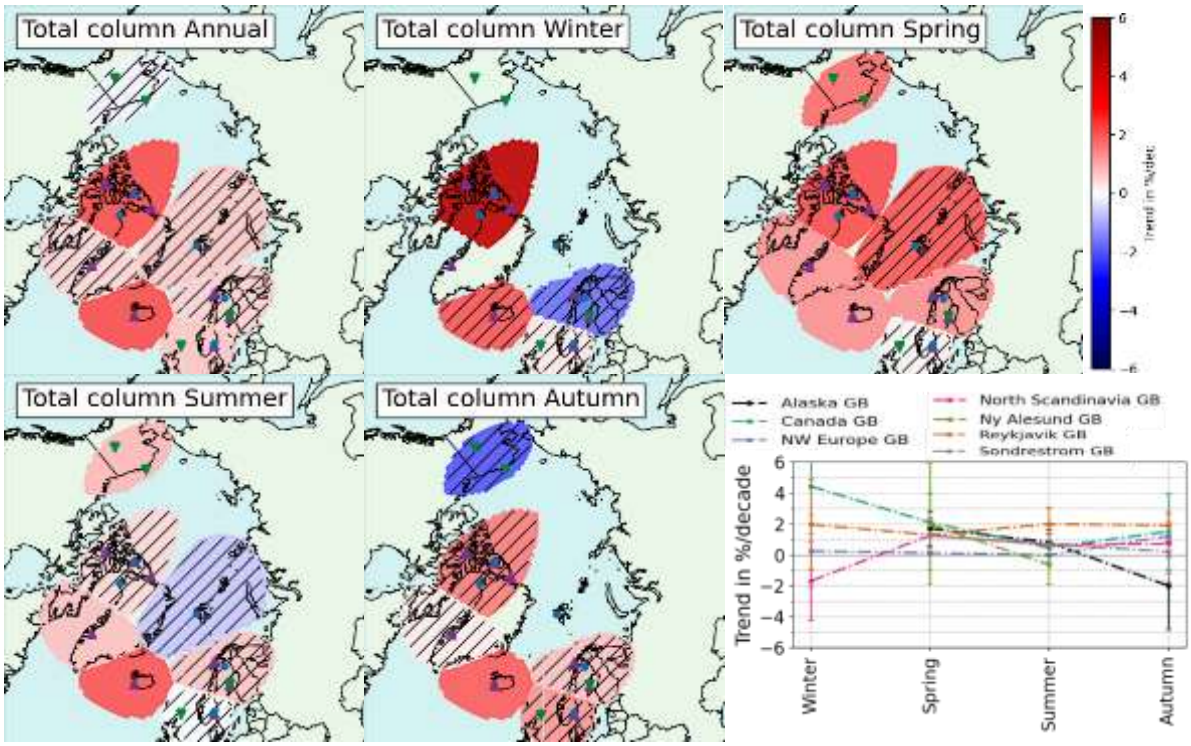

Figure 14: Annual and seasonal regional trends map for the total column of ozone. Black hatches mean the trends are not significant. Exact trend values and their 2σ uncertainties are displayed in the Annexes.

Previous studies of the total column of ozone in Arctic have found positive significant trends in individual stations. In Bernet et al. (2023), combined SAOZ, GUV and Brewer measurements led to annual positive significant trends at Andoya ($0.9 \pm 0.7\%/dec.$) and Ny-Ålesund ($1.5 \pm 1.0\%/dec.$), and a null trend at Oslo ($0.1 \pm 0.5\%/dec.$) for the 2000−2020 period. Those values agree with our results within the 2σ uncertainties. In Anjali and Kuttippurath (2025), Arctic Zonal Band total column trends based on merged SAOZ, GUV, Brewer and Dobson measurements on one hand and on merged TOMS and OMI total column ozone (MSAT) data on the other hand, are found positive and significant for the 2000−2024 period in Spring (resp. 0.75 ± 0.61 and 1.04 ± 0.85DU/year), Autumn (resp. 0.88 ± 0.23 and 0.34 ± 0.26DU/year) and annually (resp. 0.65 ± 0.39 and 0.85 ± 0.60DU/year). To

compare with literature, we calculated "zonal" trends by merging all the Arctic ground-based stations used in this work for each partial and the total column in a so-called "Arctic Zonal Band". The results are provided in the Appendix in Table D1 and compare well with Anjali and Kuttippurath (2025), although based on different instruments and methodology. Finally, we point out the significant negative ozone loss trends found in Pazmino et al. (2023) for 2000−2021 when regressing ozone loss with volume of polar stratospheric clouds for the total column of ozone using chemical transport model TOMCAT/SLIMCAT, SAOZ ground-based instruments and Multi-Sensor Reanalysis (MSR2). Without the regression with VPSC, the ozone loss trend in Pazmino et al. (2023) is not significant at the 2σ level. The VPSC detrending also lowers our total column zonal band annual trend but it remains positive and significant ($1.03 \pm 0.89\%/decade$). However, our study is based on three additional years, which can account for the difference in significance.

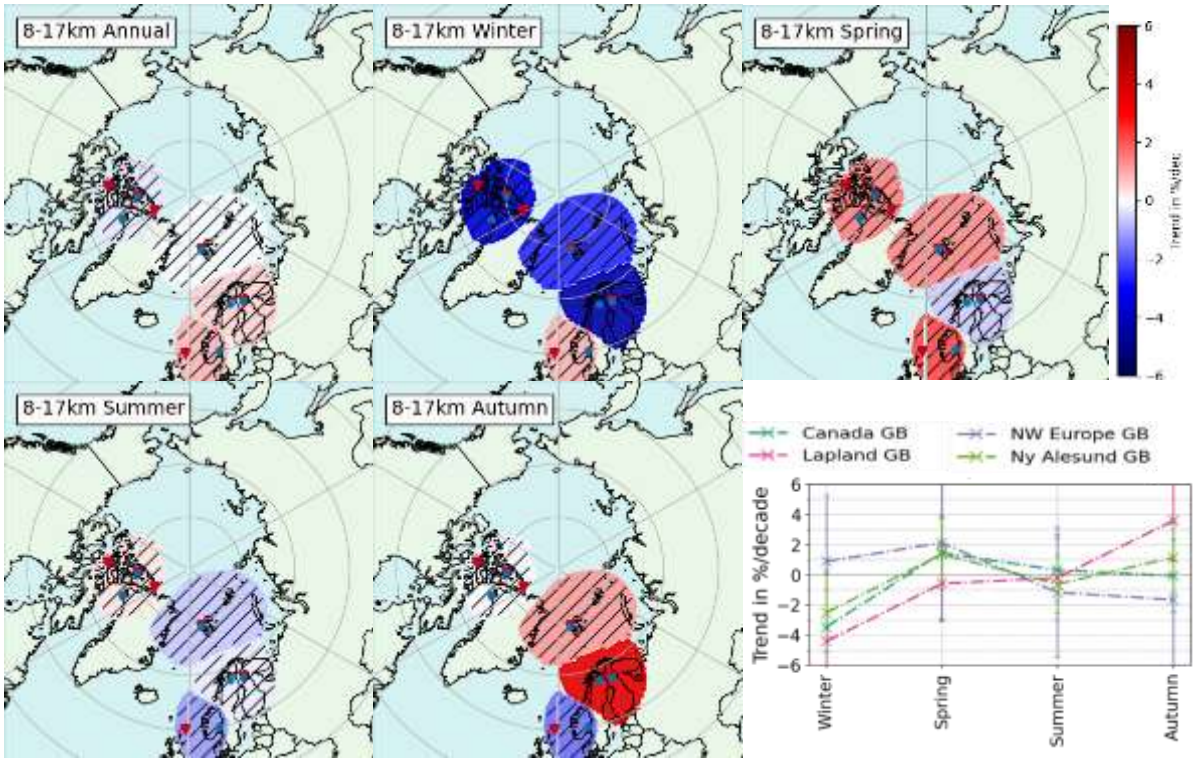

Figure 15: Same as Figure 14 for the lower stratospheric column (8-17 km) ozone trends.

We now review all partial column trends, starting with stratospheric columns. In the lower stratospheric column (8-17 km~ 300-100hPa), we find stronger seasonal and regional variations of the trends, see Figure 15. Most trends are non-significant, and they are all very small annually. They are usually strongly negative in Winter (even significantly for Lapland), and more positive in Spring. Lapland is however positive and significant in Autumn. Considering the seasonal pattern, the North-West Europe distinguishes itself from other regions with positive trends in Winter and negative trends in Autumn, although always non-significant. Lower stratospheric trends become smaller or more negative when considering the detrended VPSC proxy. This means that the positive trend in VPSC in the Arctic is delaying the expected ozone recovery in the Arctic lower stratosphere. Trends in this layer in the Arctic are reported in Nilsen et al. (2024) for individual ozonesondes as well as in Millan et al. (2025) for two satellite data sets (ACE-FTS and MLS). The former uses Dynamical Linear Modelling (DLM) to obtain time-varying trends on 20-years periods, from 1994-2014 to 2003-2023. It considers 6 Arctic stations' sondes data sets which are also used in the present work. We do not consider their Resolute and Scoresbysund results as we found spurious jumps for those data sets in section 3. At all remaining stations (Eureka, Alert, Ny-Ålesund and Sodankylä), they obtain negative annual trends within $|1\%/dec.|$ for their L2 (300-150hPa ~ 8-13 km) and L3 (150-40hPa ~ 13-22 km) layers for all periods after 1997-2017, with varying significance levels. These results are thus more negative than

ours, although they agree within 2σ errors. Besides our extended time-period and the addition of FTIR measurements, our analysis also differs in the proxies used for the regression. Nilsen et al. (2024) only considers the tropopause pressure, solar flux, Eddy heat flux (for the BDC) and the VPSC multiplied with Effective Equivalent Stratospheric Chlorine (EESC), which measures the impact of ozone-depleting stratospheric chlorine and bromine levels in the Arctic stratosphere. We have not included the EESC here because we want our trend term to reflect the impact of the declining ODS levels. Moreover, we found the temperature and equivalent latitude proxies (not included in their study) play a very important role in explaining the variability at these altitudes. The second study (Millan et al., 2025) reports overall positive annual trends around $2\%/dec$. for the MLS satellite in the 250-100hPa layer above 60ºN. These trends are not significant using a simple linear regression but become larger, positive and significant when using MLR or DLM instead. The seasonal pattern matches with ours in Winter with large negative trends and in Spring with more positive trends. In Summer we obtain negative trends contrasting their positive trends and in Autumn, we observe a strong zonal difference not captured by the latitudinal band cut of the satellite. ACE-FTS trends are highly variable (sparser sampling) but also show positive trends using MLR and DLM between 200-100hPa in the 60-70ºN latitudinal band.

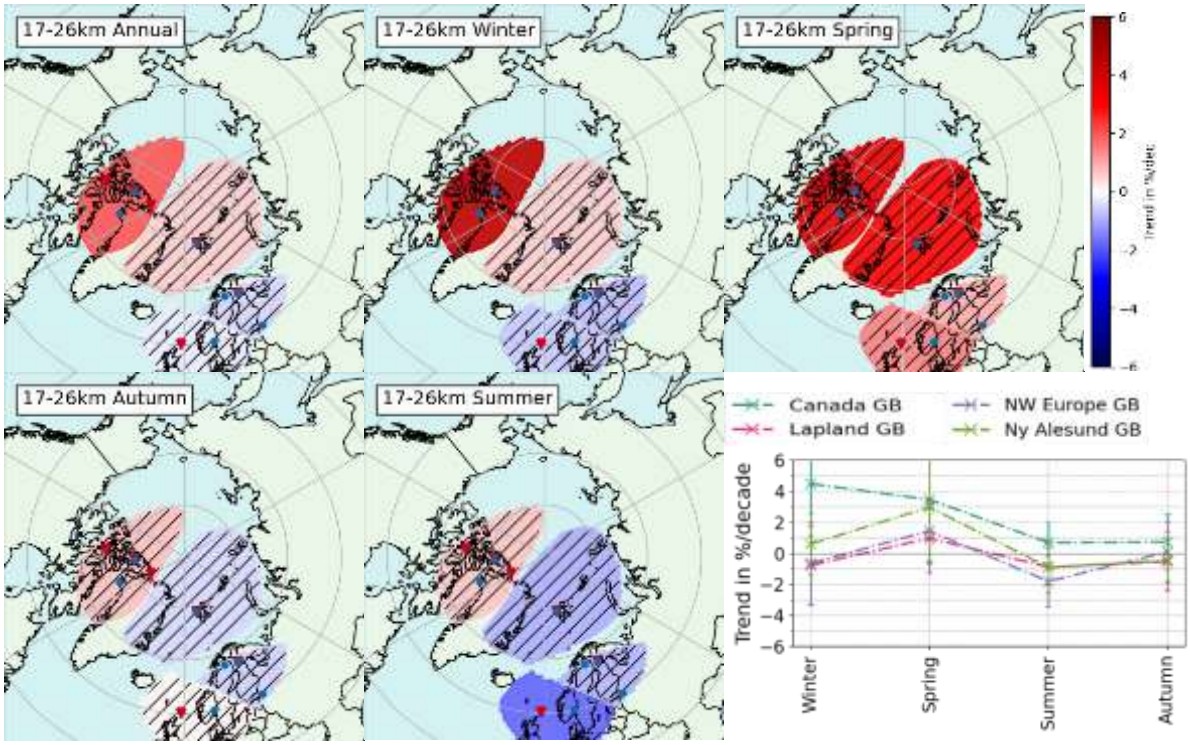

Figure 16: Same as Figure 14 for the mid stratospheric column.

In the mid-stratosphere, see Figure 16, we find positive trend values in Spring everywhere in the Arctic, while Canada trends are positive and significant in Winter and annually. There as well, the VPSC detrending lowers trends, highlighting that ozone recovery is delayed by this effect. In Sofieva et al. (2021), the annual trends at 20 km of altitude over the 2003-2018 period are very small on the whole region considered here, between -0.5 and $+1\%/dec.$, but not significant anywhere. Besides, our mid-stratospheric trends exhibit a consistent seasonal cycle, with highest (positive) ozone trends in Spring and lowest trends in Summer (significant negative in North-West Europe). The marked zonal asymmetry between Canada and Scandinavia is discussed below together with the upper stratosphere. In the upper stratosphere (Figure 17), the annual trends above North Pole are positive and significant, consistent with the results of Sofieva et al. (2021) in the 25-30 km layer and supporting the detection of ozone recovery seen in the total column trends. Seasonal trends are always non-significant; therefore, we have also considered additionally the 32-48 km layer in the Annexe. More

positive trends are generally observed at higher altitudes as in Sofieva et al. (2021) at 40 and 45 km. Indeed, we find larger positive significant trends at North Pole in Spring ($6.06 \pm 1.9\%/dec.$) and annually ($3.83 \pm 2.35\%/dec.$) for the 32-48 km layer.

In middle and upper stratosphere, we furthermore see a visible zonal asymmetry as previously detected by satellites and models (e.g. in Arosio et al., 2019; Sofieva et al., 2021) and attributed to decadal changes in the dynamics of the polar vortex above the Arctic, stemming from climate change forcing in Arosio et al. (2024). The zonal asymmetry is also visible when looking at which proxies are relevant: in the upper stratosphere, the North Pole trend is more influenced by the EL and the BDC, while the Scandinavian is driven by the EL but to a lesser extent and slightly by temperature. Similarly in the mid-stratosphere, the Canada region is the only one where the BDC plays a significant role, especially important in Spring. This hints toward an explanation of the zonal asymmetry related to the atmospheric dynamics in the Arctic, in agreement with conclusions of (Arosio et al., 2024).

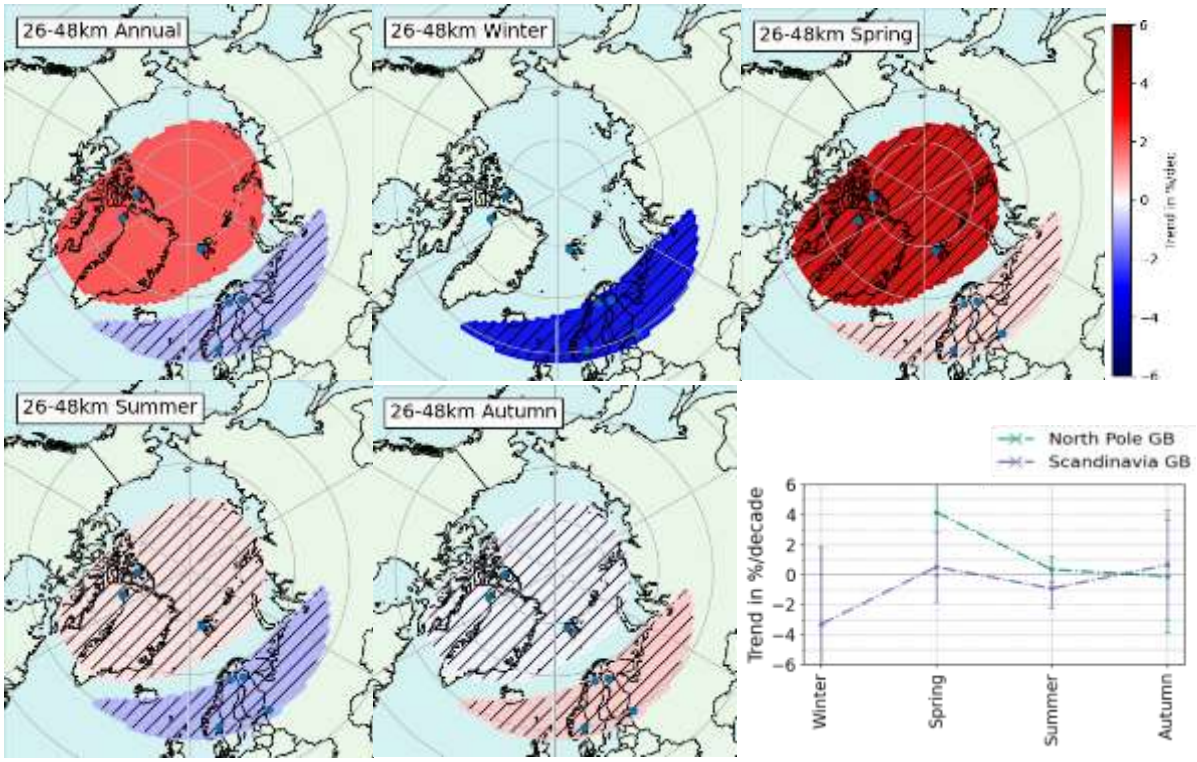

Figure 17: Same as Figure 14 for the original upper stratospheric column (26-48 km).

Next, we consider the tropospheric ozone column in Figure 18. We find that all tropospheric ozone trends are always negative in North Pole, significant both annually and in Spring, while Scandinavian trends are always non-significant, positive in Autumn and Winter and negative in Spring and Summer. In Van Malderen et al. (2025b), the HEGIFTOM measurements using homogenized sondes, FTIR, Lidar, Umkehr and IAGOS measurements lead to merged trend results on the 2000−2022 period for the tropospheric ozone column (surf.-300hPa) of (-1.80 ± 0.37)ppb/decade in their European Arctic region and of (-1.09 ± 0.57)ppb/decade in their Canadian Arctic region. For a tropospheric column of 8 km, we can approximate 1DU ~ 0.9ppb by integrating the air density column and assuming a linear decrease of temperature in the troposphere with altitude at a rate L = −0.0065K/m. This approximation will be sufficient in the context of this qualitative comparison. In North Pole (Canada+Ny-Ålesund), we find a negative but smaller annual trend of (-0.31 ± 0.27)ppb/decade at the limit of agreement with Van Malderen et al. (2025b) within mutual 2σ errors. For Scandinavia we find much smaller non-significant annual trends of (-0.04 ± 0.22)ppb/decade, not in agreement with the European Arctic value of Van Malderen et al. (2025b). The reasons for discrepancies are the exclusion of Scoresbysund (whose negative jump drives a fake negative trend when included), the addition of two years of data, and the update of FTIR data sets to the new IRWG2023 strategy. Our

seasonal trends result in the troposphere exhibit a clear seasonal cycle, with more negative values in Spring and Summer and more positive or close to zero values in Autumn and Winter. A similar seasonal cycle was observed in Law et al. (2023) for the 1995−2019 period, using ground-based measurements and models, but with a shift (maximum in Summer).

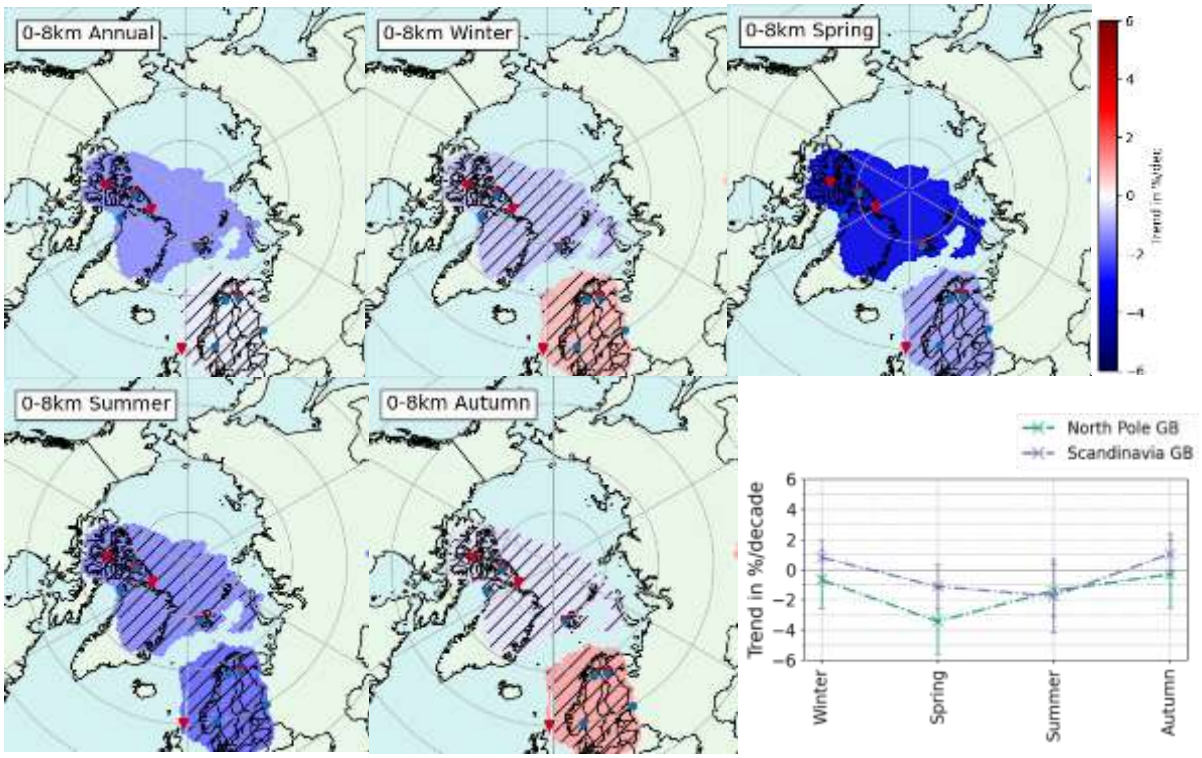

Figure 18: Same as Figure 14 for the tropospheric column 0-8 km.

Finally, we can compare the total column trends to the sum of all partial column trends to see how they match with each other and what is the individual contribution of each partial column trend to the total ozone trend, see Figure 19 and 20 for annual and seasonal trends. We sum partial column trends in DU/decade, obtained by multiplying the trends in %/decade by the mean total column value in the corresponding region. Since regions vary across partial columns, we consider equivalent regions that we have aligned vertically in Table 4 and that we name following the smallest represented regions (those of the lower stratosphere). They are Canada (North Pole in troposphere and upper stratosphere), Lapland (North Scandinavia in total column, Scandinavia in troposphere and upper stratosphere, North-East Europe in mid stratosphere), North-West Europe (Scandinavia in troposphere and upper stratosphere) and Ny-Alesund (North Pole in troposphere and upper stratosphere). In addition, we also show the zonal band mean (All Arctic). Our first conclusion is that the impact of tropospheric trends is very small in DU/decade over the whole total column trend budget. We find overall agreement within the error bars of the total column trend and the sum of partial columns trends. This is a nontrivial feature since the various columns use measurements from different sets of instruments and give confidence in our methodology. The best match of sums of partial column trends to total column trends is observed in Spring, comforting the results of ozone recovery at that season. In Ny-Ålesund in particular, the total column trend and the sum of partial columns trends agree very well both annually and for all seasons, although the upper stratospheric and total column trends are only given by the FTIR dataset while the three lower partial columns are a merging of the ozonesondes and FTIR data sets, see Table 2.

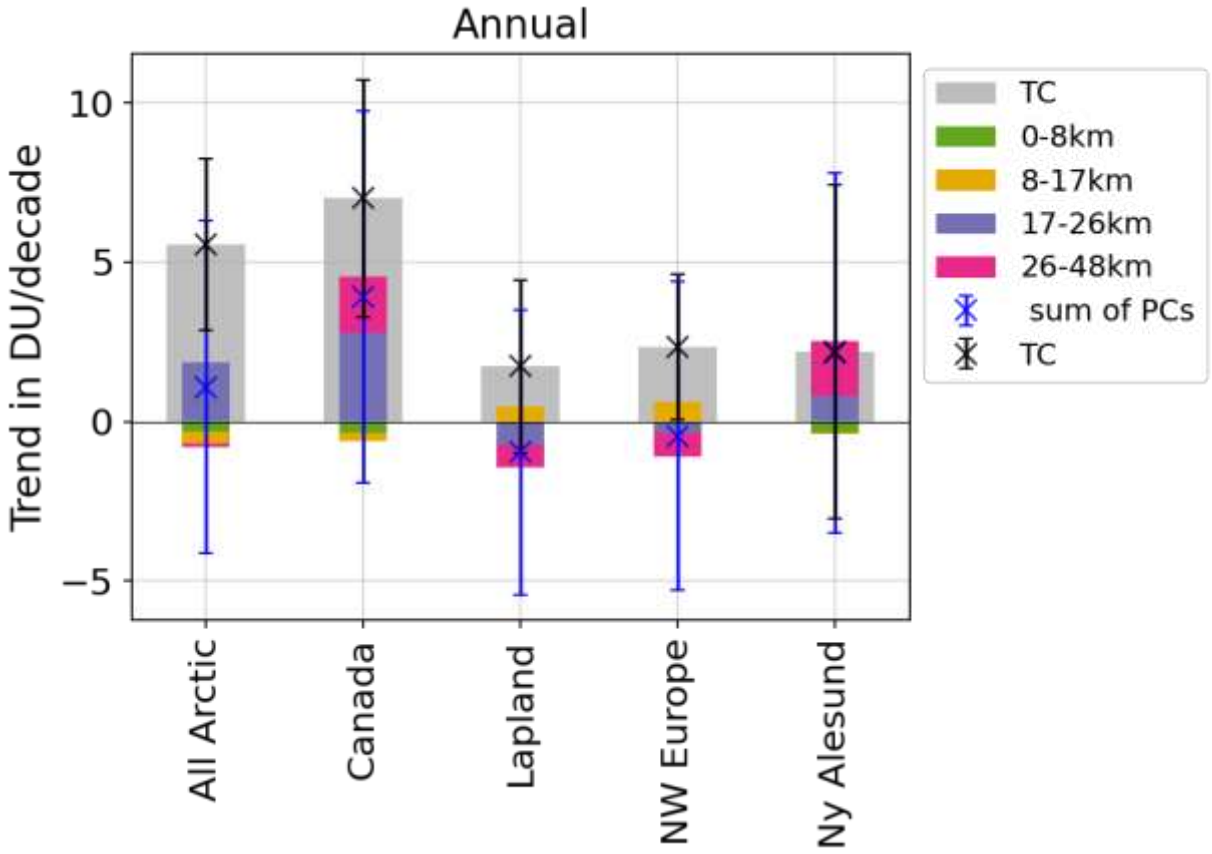

Figure 19: Sums of all partial columns trends compared to total column trends in DU per decade for annual trends. The groups are not always the same across the different layers, therefore we calculate sums for the smallest represented regions, i.e., the regions of the lower stratosphere (8-17 km). As shown in Table 4, we have for instance: **Canada** (TC) = North Pole (0-8 km) + Canada (8-17 km) + Canada (17-26 km) + North Pole (26-48 km) and **North Scandinavia** (TC) = Scandinavia (0-8 km) + Lapland (8-17 km) + North-East Europe (17-26 km) + Scandinavia (26-48 km).

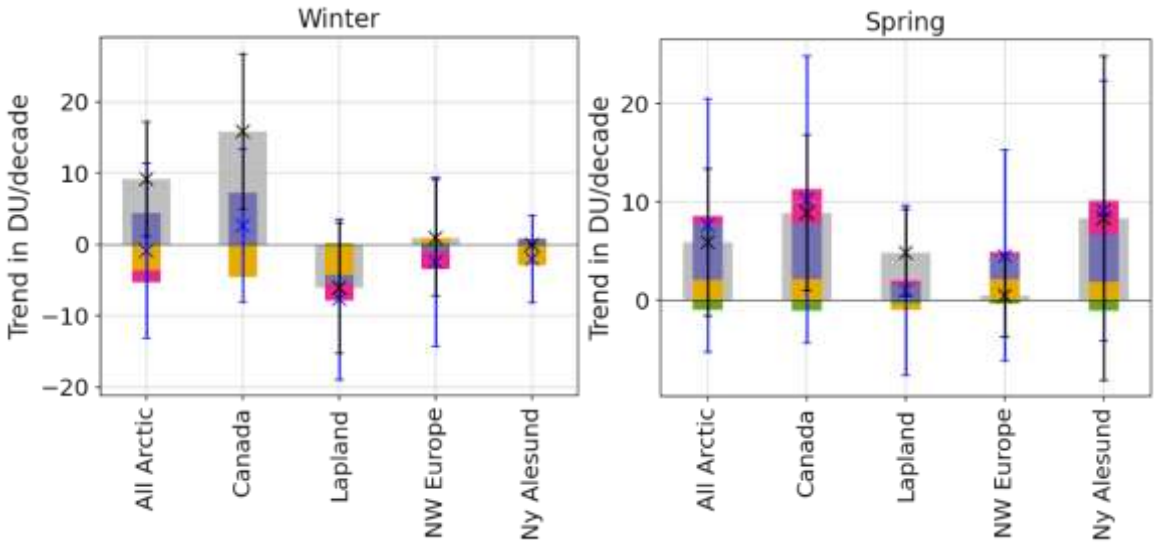

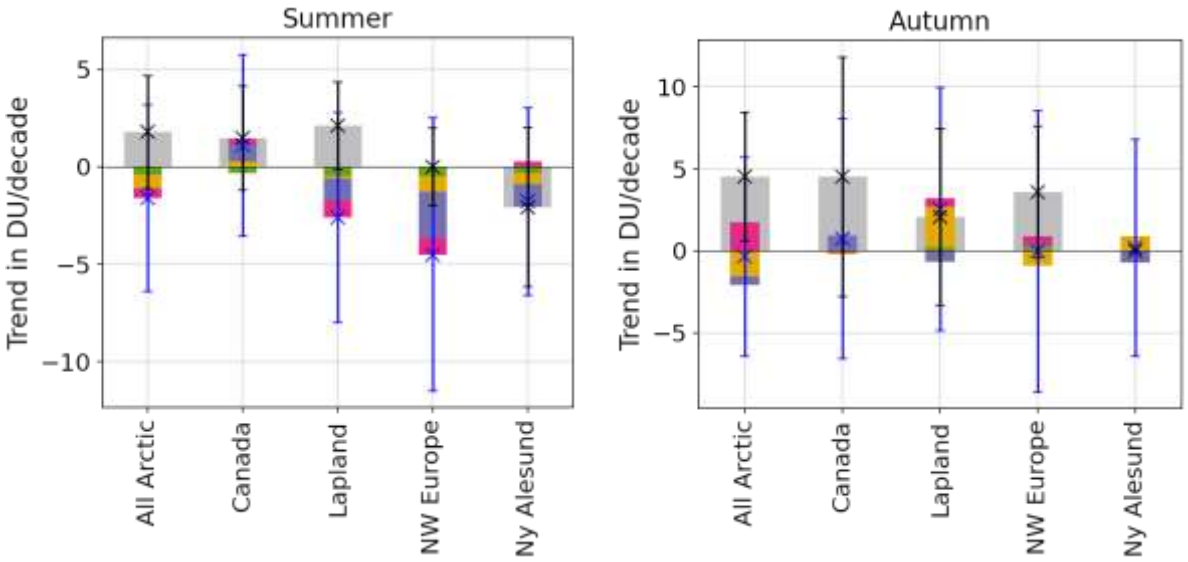

Figure 20: Same as Figure 19 for all seasonal trends.

CONCLUSIONS

By conducting a representativeness analysis based on CAMS re-analysis ozone profiles, we identified spatially coherent regions in which the combined time series yield reduced uncertainties and robust trend estimates for the total column as well as for four vertically resolved partial columns covering the troposphere and stratosphere (0–48 km), while enabling a finer description of ozone's evolution than zonal bands.

Cross-comparison with IASI-CDR and MEGRIDOP revealed only minor drifts (< 3%/dec) in those satellite products, consistent with satellite's stability requirements (Weber, 2024), while it enabled us to exclude problematic ground-based data sets from our trend analysis.

Using a stepwise multiple-linear regression, incorporating nine physical proxies (solar cycle, QBO, ENSO, Arctic Oscillation, Brewer–Dobson circulation, equivalent latitude, stratospheric temperature, tropopause pressure and volume of polar stratospheric clouds) we can detect ozone recovery (over the 2000–2024 period) due to ODS depletion while attributing ozone's variability to those physical processes. The obtained annual trends indicate a positive evolution of ozone total columns over the Arctic, statistically significant over Canada, Reykjavik (both +2.1%/dec), and North-West Europe (+0.7%/dec). We also detect an ozone recovery annually over the Canada region (+2%/dec) in the mid-stratosphere (17–26 km) and over the North Pole region (Canada + Ny-Ålesund) in the upper stratosphere (+2.1%/dec for 26–48 km and +3.8%/dec for 32–48 km). Those trends are more pronounced in Spring. Elsewhere and in the lower stratospheric column, trends are small and not significant. Even when non-significant, we see consistent seasonal patterns: e.g., trends are usually negative in Winter in the lower stratosphere (significantly for Lapland), and in Summer for the mid-stratosphere. The zonal asymmetry observed e.g., in Arosio et al. (2019); Sofieva et al. (2021) for the middle and upper stratosphere is also visible in our results.

By analysing the proxies' influences, we find that equivalent latitude, temperature and volume of polar stratospheric clouds dominate the variability budget in stratospheric columns. The tropopause pressure plays a significant role in explaining the variability for single-site regions. We also see a slow down of the expected ozone recovery especially in the lower stratosphere (but also regionally in upper layers) due to stratospheric cooling ($-0.6\%/decade$) and the increase of volume of polar stratospheric clouds ($-0.8\%/decade$).

Annual tropospheric ozone trends are negative in the North Pole region (Canada+Ny-Ålesund), but non-significant in Scandinavia. The tropospheric trends are more negative in Spring: -1.1%/dec in Scandinavia and -3.4%/dec (significant) in North Pole. The impact of the tropospheric trends is found to be negligible in the total column trend budget, as visible from the comparison of sums of partial columns versus total column trends.

Our study highlights the importance of long-term data sets of ozone measurements obtained simultaneously from a variety of ground-based instruments. Although ozone recovery starts to be observed in the Arctic, a continued monitoring is necessary to further assess the impact of climate change, which may undermine the efforts undertaken since the Montreal Protocol agreement, despite the successful reduction of ozone-depleting substances worldwide.

5. DISSEMINATION AND VALORISATION

DORA WEBSITE

A website (https://dora.aeronomie.be/) has been implemented and updated during the project with scientific communications and results. The generated data (VPSC proxy, merged time-series,…) are also made available there (Jan. 2026).

GENERAL PUBLIC

Presentation of the DORA project at 3 primary schools and general public during the WiseNight 2025 organised by BeWise and Soapbox Science, at the Brussels Planetarium, 26th Sept. 2025.

SCIENTIFIC COMMUNICATION

In addition to DORA annual meetings with following-up committee members, this project has been presented in several conferences (all presentations can be found in the DORA website https://dora.aeronomie.be/index.php/progress):

- ACTRIS Science Conference in Rennes 13-16 May 2024
  Talk in the session on *Long-term trends and variability of the atmospheric composition*.
- DORA midterm evaluation 10 June 2024, online meeting in front of the following-up committee members and Belspo representative
  Presented results, progress, and prospects of the project
- NDACC/IRWG-TCCON-COCCON annual meeting in Boulder, Colorado 8-12 July 2024
  Talk in the NDACC/IRWG session
- Quadrennial Ozone Symposium in Boulder, Colorado 14-19 July 2024
  Talk in the session on *Stratospheric Ozone Science*
- European Geosciences Union General Assembly in Vienna, Austria 28 April-2 May 2025
  PICO presentation in the session on *Atmospheric composition variability and trends*
- BE-Polar Conference in Brussels, 11th September 2025
  Talk in the *Atmospheric Science* session
- NDACC Symposium 2025, Virginia Beach, VA , USA, 27-30 October 2025
  Online Poster
- DORA final meeting, November 2025, online meeting in front of the following-up committee members and Belspo representative
  Final results of the project

- Our involvement in LOTUS as the FTIR representative and our constant contact with NDACC PIs has led to updated FTIR data sets (“strategy “irwg2023”), used in Viktoria et al., 2025.
- Our involvement in TOAR-II as the FTIR representative led to the inclusion of FTIR in the global ozone tropospheric trend study from Van Malderen et al., 2025a.
- The tool developed for our representativeness study has been valorised in TOAR-II / HEGIFTOM for regional ozone tropospheric trends (Van Malderen, 2025b).
- Our involvement in LOTUS as the FTIR representative led to the LOTUS publication on ground-based regional trends (over the globe) using partial columns (Mirallie et al., submitted 2026). Our tool on representativeness was also used in this paper.

6. PUBLICATIONS

Jonas, C., Vigouroux, C., Langerock, B., Björklund, R., Boynard, A., Carlund, T., De Mazière, M., Effertz, P., Errera, Q., Frey, M., Hannigan, J. W., Jepsen, N., Kivi, R., Lyall, N., Palm, M., Prignon, M., Sofieva, V. F., Strong, K., Svendby, T., Tarasick, D., Thölix, L., Van Malderen, R., Virolainen, Y., von Löwis, S., and Zhao, X.: Detection of ozone recovery in the Arctic from ground-based measurements, EGUsphere [preprint], https://doi.org/10.5194/egusphere-2025-6473, 2026.

Mirallie, Louis, Eliane Maillard Barras, Caroline Jonas, Corinne Vigouroux, Roeland Van Malderen, Irina Petropavlovskikh, Sophie Godin-Beekmann, Thierry Leblanc, Wolfgang Steinbrecht, Antoine Vadès, Rolf Ruefenach, Alexander Haefele, Gunter Stober, Peter Effertz, Julian Gröbner, Gerard Ancellet, María Cazorla, Petra Duff, Matthias Frey, Michael Gill, James W. Hannigan, Nicholas Jones, Rigel Kivi, Raphael Koehler, Bogumil Kois, Debra Kollonige, Emmanuel Mahieu, Glen McConville, Johan Mellqvist, Gary Morris, Isao Murata, Tomoo Nagahama, Gerald E. Nedoluha, Shin-Ya Ogino, Richard Querel, Ryan Stauffer, Wolfgang Stremme, Kimberly Strong, Ralf Sussmann, Anne Thompson, and Yana Virolainen: Ozone stratospheric trends from regional bayesian composite of ground-based partial columns, submitted to ACP, 2026.

Sofieva, V. F., Szelag, M. E., Kramarova, N., Damadeo, R., Steinbrecht, W., Petropavlovskikh, I., Vigouroux, C., Maillard Barras, E., Zawada, D., Tourpali, K., Frith, S. M., Wild, J. D., Davis, S. M., Arosio, C., Weber, M., Rozanov, A., Auffarth, B., Froidevaux, L., Fuller, R., Degenstein, D., Dube, K., Effertz, P., Leblanc, T., Ancellet, G., Godin-Beekmann, S., McConville, G., Querel, R., Smale, D., DeBacker, M.-R., Mahieu, E., and Sussmann, R.: Updated global and regional trends of stratospheric ozone profiles, EGUsphere [preprint], https://doi.org/10.5194/egusphere-2025-5963, 2025.

Van Malderen, R., Zang, Z., Chang, K.-L., Björklund, R., Cooper, O. R., Liu, J., Maillard Barras, E., Vigouroux, C., Petropavlovskikh, I., Leblanc, T., Thouret, V., Wolff, P., Effertz, P., Gaudel, A., Tarasick, D. W., Smit, H. G. J., Thompson, A. M., Stauffer, R. M., Kollonige, D. E., Poyraz, D., Ancellet, G., De Backer, M.-R., Frey, M. M., Hannigan, J. W., Hernandez, J. L., Johnson, B. J., Jones, N., Kivi, R., Mahieu, E., Morino, I., McConville, G., Müller, K., Murata, I., Notholt, J., Piters, A., Prignon, M., Querel, R., Rizi, V., Smale, D., Steinbrecht, W., Strong, K., and Sussmann, R.: Ground-based tropospheric ozone measurements: regional tropospheric ozone column trends from the TOAR-II/HEGIFTOM homogenized datasets, Atmos. Chem. Phys., 25, 9905–9935, https://doi.org/10.5194/acp-25-9905-2025, 2025.

Van Malderen, R., Thompson, A. M., Kollonige, D. E., Stauffer, R. M., Smit, H. G. J., Maillard Barras, E., Vigouroux, C., Petropavlovskikh, I., Leblanc, T., Thouret, V., Wolff, P., Effertz, P., Tarasick, D. W., Poyraz, D., Ancellet, G., De Backer, M.-R., Evan, S., Flood, V., Frey, M. M., Hannigan, J. W., Hernandez, J. L., Iarlori, M., Johnson, B. J., Jones, N., Kivi, R., Mahieu, E., McConville, G., Müller, K., Nagahama, T., Notholt, J., Piters, A., Prats, N., Querel, R., Smale, D., Steinbrecht, W., Strong, K., and Sussmann, R.: Global ground-based tropospheric ozone measurements: reference data and individual site trends (2000–2022) from the TOAR-II/HEGIFTOM project, Atmos. Chem. Phys., 25, 7187–7225, https://doi.org/10.5194/acp-25-7187-2025, 2025.

7. ACKNOWLEDGEMENTS

The FTIR, Brewer, Dobson, and ozonesonde principal investigators and staff at the stations (NDACC, WOUDC) included in the work are warmly thanked for the provision of high-quality reference measurements. Specifically, we thank Petra Duff and Ivan Ortega for the Eureka and Thule FTIR IRWG2023 retrievals, respectively, and Johan Mellqvist and Frank Hase as PIs for the Harestua and Kiruna stations, respectively.

We thank all the co-authors who contributed, gave comments and helped to improve the quality of the paper written from this project. We also thank the members of the following-up committee for discussion and support.

ANNEXES

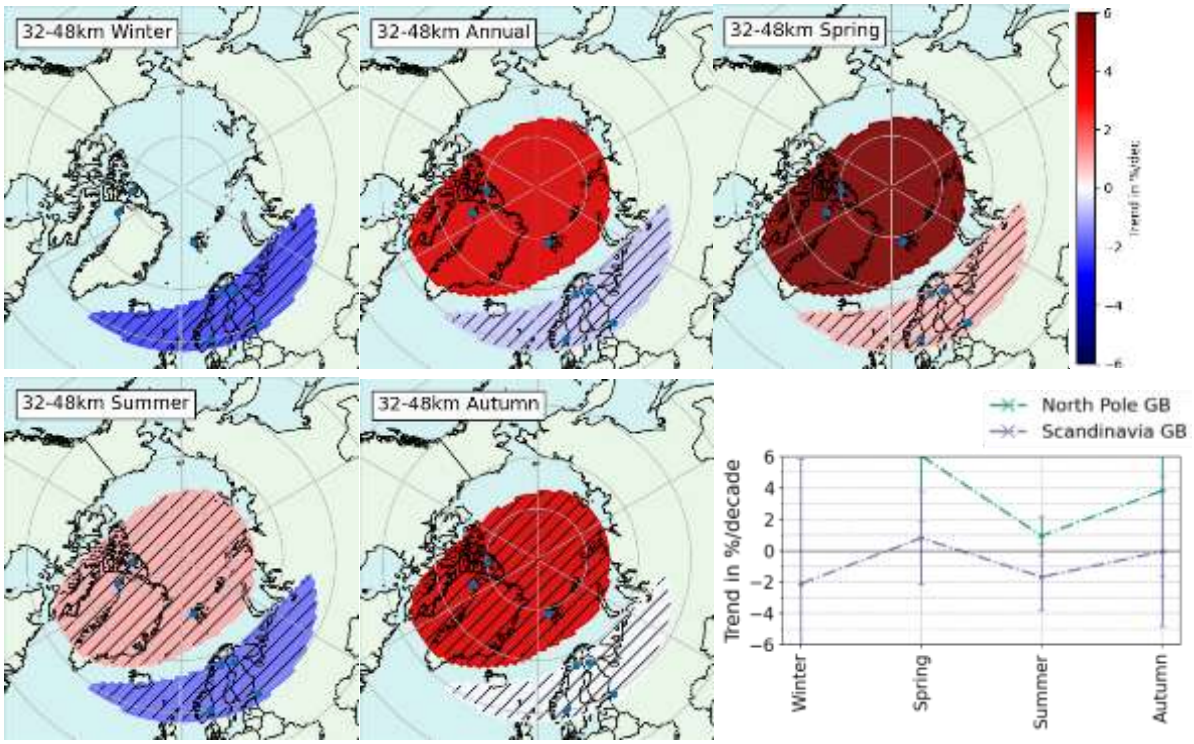

Figure A1: Annual and seasonal trends in the alternative upper stratospheric column (32-48 km)

Region	Season	TC (%/dec.)	(DU/dec.)	Region	Season	TC (%/dec.)	(DU/dec.)
Arctic Zonal Band	Annual	**1.67 ± 0.81**	**5.56 ± 2.69**	North Scandinavia	Annual	0.53 ± 0.84	1.73 ± 2.72
	Winter	**2.63 ± 2.29**	**9.2 ± 8.02**		Winter	-1.68 ± 2.54	-6.07 ± 9.16
	Spring	1.42 ± 1.81	5.89 ± 7.5		Spring	**1.27 ± 1.17**	**4.83 ± 4.46**
	Summer	0.55 ± 0.9	1.78 ± 2.9		Summer	0.66 ± 0.71	2.1 ± 2.24
	Autumn	**1.54 ± 1.34**	**4.52 ± 3.93**		Autumn	0.72 ± 1.88	2.06 ± 5.4
Canada	Annual	**2.07 ± 1.1**	**7.01 ± 3.73**	Alaska	Annual	-0.11 ± 1.02	-0.36 ± 3.47
	Winter	**4.44 ± 3.06**	**15.85 ± 10.92**				
	Spring	**2.1 ± 1.87**	**8.91 ± 7.91**		Spring	**1.72 ± 1.13**	**6.86 ± 4.51**
	Summer	0.47 ± 0.85	1.48 ± 2.69		Summer	**0.82 ± 0.81**	**2.64 ± 2.6**
	Autumn	1.52 ± 2.45	4.53 ± 7.3		Autumn	-1.98 ± 2.85	-6.0 ± 8.65
North-West Europe	Annual	**0.7 ± 0.68**	**2.34 ± 2.28**	Reykjavik	Annual	**2.09 ± 0.85**	**7.13 ± 2.89**
	Winter	0.26 ± 2.36	0.88 ± 8.14		Winter	1.98 ± 2.91	6.67 ± 9.83
	Spring	0.13 ± 1.09	0.49 ± 4.18		Spring	**1.31 ± 0.89**	**5.1 ± 3.48**
	Summer	-0.0 ± 0.6	-0.0 ± 1.99		Summer	**2.0 ± 1.08**	**6.94 ± 3.74**
	Autumn	1.22 ± 1.37	3.57 ± 4.01		Autumn	**1.92 ± 0.87**	**5.63 ± 2.56**
Ny-Ålesund	Annual	0.63 ± 1.49	2.19 ± 5.23	Sondrestrom	Annual	0.51 ± 0.74	1.73 ± 2.52
	Spring	1.99 ± 3.91	8.37 ± 16.48		Spring	**1.25 ± 1.01**	**4.99 ± 4.05**
	Summer	-0.63 ± 1.25	-2.07 ± 4.09		Summer	**0.71 ± 0.61**	**2.34 ± 2.04**
					Autumn	0.22 ± 1.93	0.67 ± 5.9

Table A1: Annual and seasonal total column trends obtained from our ground-based regionally merged data sets with 2σ uncertainties, given both in percent per decade and in DU per decade. Significant trends are highlighted in bold. Missing seasons such as Ny-Alesund Winter and Autumn mean that the number of available points in the time series was considered too small for applying the regression (we use a fixed threshold of at least 80 data points for annual trends and at least 25 points for seasonal trends). Partial column trends are presented in Tables A2, A3.

Region	Season	8 – 17km		17 – 26km	
		%/dec.	DU/dec.	%/dec.	DU/dec.
Arctic	Annual	-0.41 ± 1.45	-0.4 ± 1.42	1.33 ± 1.52	1.87 ± 2.13
Zonal	Winter	-3.0 ± 3.75	-3.47 ± 4.33	$\mathbf{2.88 \pm 2.76}$	$\mathbf{4.47 \pm 4.29}$
Band	Spring	1.64 ± 2.38	2.11 ± 3.05	3.55 ± 4.33	5.66 ± 6.9
	Summer	-0.81 ± 1.98	-0.67 ± 1.64	-0.04 ± 1.56	-0.05 ± 1.97
	Autumn	-2.0 ± 2.01	-1.53 ± 1.55	-0.42 ± 1.52	-0.54 ± 1.95
Canada	Annual	-0.26 ± 1.58	-0.28 ± 1.69	$\mathbf{2.01 \pm 1.54}$	$\mathbf{2.79 \pm 2.14}$
	Winter	-3.47 ± 3.8	-4.41 ± 4.83	$\mathbf{4.49 \pm 3.36}$	$\mathbf{7.23 \pm 5.42}$
	Spring	1.47 ± 2.44	2.16 ± 3.59	3.47 ± 4.14	5.62 ± 6.7
	Summer	0.32 ± 2.11	0.29 ± 1.9	0.7 ± 1.31	0.87 ± 1.64
	Autumn	-0.06 ± 2.4	-0.05 ± 2.09	0.75 ± 1.77	0.95 ± 2.25
Ny-Ålesund	Annual	-0.04 ± 1.56	-0.04 ± 1.55	0.58 ± 1.53	0.8 ± 2.1
	Winter	-2.52 ± 2.6	-2.72 ± 2.8	0.6 ± 1.97	0.86 ± 2.82
	Spring	1.39 ± 2.37	1.85 ± 3.15	2.98 ± 3.58	4.82 ± 5.79
	Summer	-0.61 ± 1.87	-0.54 ± 1.65	-0.91 ± 1.57	-1.18 ± 2.04
	Autumn	1.15 ± 2.33	0.9 ± 1.83	-0.44 ± 1.39	-0.57 ± 1.81
Lapland/	Annual	0.98 ± 1.55	0.81 ± 1.3	-0.49 ± 1.02	-0.67 ± 1.39
North-East	Winter	$\mathbf{-4.43 \pm 3.31}$	$\mathbf{-4.26 \pm 3.18}$	-0.77 ± 2.56	-1.16 ± 3.87
Europe	Spring	0.02 ± 2.23	0.02 ± 2.4	0.97 ± 2.23	1.53 ± 3.51
	Summer	0.91 ± 2.24	0.64 ± 1.58	-0.87 ± 1.19	-1.1 ± 1.5
	Autumn	$\mathbf{4.15 \pm 2.71}$	$\mathbf{2.71 \pm 1.77}$	-0.53 ± 1.9	-0.66 ± 2.39
North-West	Annual	0.85 ± 2.33	0.63 ± 1.72	-0.23 ± 1.03	-0.32 ± 1.43
Europe	Winter	0.89 ± 4.4	0.74 ± 3.66	-0.64 ± 2.67	-0.98 ± 4.12
	Spring	2.14 ± 5.19	2.15 ± 5.22	1.46 ± 1.91	2.28 ± 3.0
	Summer	-1.16 ± 4.31	-0.81 ± 2.98	$\mathbf{-1.8 \pm 1.63}$	$\mathbf{-2.35 \pm 2.12}$
	Autumn	-1.64 ± 5.21	-0.91 ± 2.88	0.1 ± 1.94	0.12 ± 2.46

Table A2: Lower and mid stratospheric regional trends in %/decade and DU/decade with 2σ uncertainties. Significant trends in bold.

Region	Season	0 – 8km		26 – 48km		32 – 48km	
		%/dec.	DU/dec.	%/dec.	DU/dec.	%/dec.	DU/dec.
Arctic	Annual	**-1.19 ± 1.08**	**-0.3 ± 0.27**	-0.1 ± 1.71	-0.08 ± 1.39	-0.26 ± 2.4	-0.09 ± 0.81
Zonal	Winter	-0.51 ± 1.56	-0.12 ± 0.38	-2.33 ± 4.44	-1.72 ± 3.28	-1.67 ± 6.63	-0.44 ± 1.75
Band	Spring	**-3.04 ± 2.04**	**-0.93 ± 0.63**	0.89 ± 2.6	0.79 ± 2.29	0.69 ± 2.83	0.25 ± 1.01
	Summer	-1.64 ± 1.69	-0.41 ± 0.43	-0.54 ± 0.87	-0.47 ± 0.74	-1.5 ± 1.55	-0.6 ± 0.61
	Autumn	-0.11 ± 1.77	-0.03 ± 0.42	2.29 ± 2.87	1.73 ± 2.17	1.93 ± 4.55	0.59 ± 1.39
Scandinavia	Annual	-0.2 ± 0.98	-0.05 ± 0.25	-0.85 ± 1.71	-0.72 ± 1.44	-0.62 ± 2.71	-0.22 ± 0.95
	Winter	0.81 ± 1.2	0.19 ± 0.28	-3.3 ± 5.11	-2.44 ± 3.78	-2.12 ± 7.95	-0.55 ± 2.08
	Spring	-1.12 ± 1.44	-0.33 ± 0.42	0.51 ± 2.34	0.46 ± 2.09	0.8 ± 2.98	0.29 ± 1.08
	Summer	-1.74 ± 2.41	-0.47 ± 0.65	-0.92 ± 1.3	-0.88 ± 1.25	-1.68 ± 2.14	-0.7 ± 0.88
	Autumn	1.05 ± 1.36	0.24 ± 0.31	0.65 ± 3.67	0.52 ± 2.93	-0.06 ± 4.76	-0.02 ± 1.56
North	Annual	**-1.33 ± 1.15**	**-0.34 ± 0.3**	**2.15 ± 2.08**	**1.75 ± 1.7**	**3.83 ± 2.35**	**1.32 ± 0.81**
Pole	Winter	-0.67 ± 1.91	-0.17 ± 0.49				
	Spring	**-3.43 ± 2.16**	**-1.07 ± 0.68**	4.15 ± 4.25	3.52 ± 3.6	**6.06 ± 4.19**	**2.11 ± 1.46**
	Summer	-1.38 ± 1.71	-0.33 ± 0.41	0.35 ± 0.85	0.29 ± 0.71	0.94 ± 1.23	0.35 ± 0.45
	Autumn	-0.31 ± 2.24	-0.08 ± 0.55	-0.11 ± 3.76	-0.07 ± 2.43	3.82 ± 5.48	0.96 ± 1.37

Table A3: Tropospheric and upper stratospheric regional trends in %/decade and DU/decade with 2σ uncertainties. Significant trends in bold.

References:

- Anjali, S. and Kuttippurath, J.: Tracing the signatures of ozone recovery in the Arctic ozone, Scientific Reports, 15, 35 304, https://doi.org/10.1038/s41598-025-19373-0, 2025.
- Arosio, C., Rozanov, A., Malinina, E., Weber, M., and Burrows, J. P.: Merging of ozone profiles from SCIAMACHY, OMPS and SAGE II observations to study stratospheric ozone changes, Atmospheric Measurement Techniques, 12, 2423–2444, https://doi.org/10.5194/amt-12-2423-2019, 2019.
- Arosio, C., Chipperfield, M. P., Rozanov, A., Weber, M., Dhomse, S., Feng, W., Jaross, G., Zhou, X., and Burrows, J. P.: Investigating Zonal Asymmetries in Stratospheric Ozone Trends From Satellite Limb Observations and a Chemical Transport Model, Journal of Geophysical Research: Atmospheres, 129, e2023JD040 353, https://doi.org/https://doi.org/10.1029/2023JD040353, e2023JD040353 2023JD040353, 2024.
- Ball, W. T., Alsing, J., Mortlock, D. J., Staehelin, J., Haigh, J. D., Peter, T., Tummon, F., Stubi, R., Stenke, A., Anderson, J., Bourassa, A., Davis, S. M., Degenstein, D., Frith, S., Froidevaux, L., Roth, C., Sofieva, V., Wang, R., Wild, J., Yu, P., Ziemke, J. R., and Rozanov, E. V.: Evidence for a continuous decline in lower stratospheric ozone offsetting ozone layer recovery, Atmospheric Chemistry and Physics, 18, 1379–1394, https://doi.org/10.5194/acp-18-1379-2018, 2018.
- Barnett, J. J., Houghton, J. T., and Pyle, J. A.: The temperature dependence of the ozone concentration near the stratopause, Quarterly Journal of the Royal Meteorological Society, 101, 245–257, https://doi.org/https://doi.org/10.1002/qj.49710142808, 1975.
- Benito-Barca, S., Abalos, M., Calvo, N., Garny, H., Birner, T., Abraham, N. L., Akiyoshi, H., Dennison, F., Jockel, P., Josse, B., Keeble, J., Kinnison, D., Marchand, M., Morgenstern, O., Plummer, D., Rozanov, E., Strode, S., Sukhodolov, T., Watanabe, S., and Yamashita, Y.: Recent Lower Stratospheric Ozone Trends in CCMI-2022 Models: Role of Natural Variability and Transport, Journal of Geophysical Research: Atmospheres, 130, e2024JD042 412, https://doi.org/https://doi.org/10.1029/2024JD042412, e2024JD042412 2024JD042412, 2025.

- Bernet, L., Svendby, T., Hansen, G., Orsolini, Y., Dahlback, A., Goutail, F., Pazmino, A., Petkov, B., and Kylling, A.: Total ozone trendsat three northern high-latitude stations, Atmospheric Chemistry and Physics, 23, 4165–4184, https://doi.org/10.5194/acp-23-4165-2023, 2023.
- Bjorklund, R., Vigouroux, C., Effertz, P., Garcia, O. E., Geddes, A., Hannigan, J., Miyagawa, K., Kotkamp, M., Langerock, B., Nedoluha, G., Ortega, I., Petropavlovskikh, I., Poyraz, D., Querel, R., Robinson, J., Shiona, H., Smale, D., Smale, P., Van Malderen, R., and De Maziere, M.: Intercomparison of long-term ground-based measurements of total, tropospheric, and stratospheric ozone at Lauder, New Zealand, Atmospheric Measurement Techniques, 17, 6819–6849, https://doi.org/10.5194/amt-17-6819-2024, 2024.
- Boynard, A., Wespes, C., Hadji-Lazaro, J., Sinnathamby, S., Hurtmans, D., Coheur, P.-F., Doutriaux-Boucher, M., Onderwaater, J., Steinbrecht, W., Pennington, E. A., Bowman, K., and Clerbaux, C.: Assessment of 16-year tropospheric ozone trends from the IASI Climate Data Record, Atmospheric Chemistry and Physics, 25, 11 719–11 755, https://doi.org/10.5194/acp-25-11719-2025, 2025.
- Brasseur, G. P. and Solomon, S.: Aeronomy of the middle atmosphere, Atmospheric and Oceanographic Sciences Library, Springer, New York, NY, 3 edn., 2005.
- Brunner, D., Staehelin, J., Maeder, J. A., Wohltmann, I., and Bodeker, G. E.: Variability and trends in total and vertically resolved stratospheric ozone based on the CATO ozone data set, Atmospheric Chemistry and Physics, 6, 4985–5008, https://doi.org/10.5194/acp-6-4985-2006, 2006.
- Chipperfield, M. P., Dhomse, S., Hossaini, R., Feng, W., Santee, M. L., Weber, M., Burrows, J. P., Wild, J. D., Loyola, D., and Coldewey-Egbers, 685 M.: On the Cause of Recent Variations in Lower Stratospheric Ozone, Geophysical Research Letters, 45, 5718–5726, https://doi.org/https://doi.org/10.1029/2018GL078071, 2018.
- Christiansen, B., Jepsen, N., Kivi, R., Hansen, G., Larsen, N., and Korsholm, U. S.: Trends and annual cycles in soundings of Arctic tropospheric ozone, Atmospheric Chemistry and Physics, 17, 9347–9364, https://doi.org/10.5194/acp-17-9347-2017, 2017.
- Clerbaux, C. and Coheur, P.-F.: Daily IASI/Metop-A ULB-LATMOS ozone (O3) L2 product (vertical profile and columns – EUMETSAT processing), https://doi.org/10.25326/806, 2025a.
- Clerbaux, C. and Coheur, P.-F.: Daily IASI/Metop-B ULB-LATMOS ozone (O3) L2 product (vertical profile and columns – EUMETSAT processing), https://doi.org/10.25326/807, 2025b.
- Coldewey-Egbers, M., Loyola, D. G., Lerot, C., and Van Roozendael, M.: Global, regional and seasonal analysis of total ozone trends derived from the 1995–2020 GTO-ECV climate data record, Atmospheric Chemistry and Physics, 22, 6861–6878, https://doi.org/10.5194/acp-695 22-6861-2022, 2022.
- Cooper, O. R., Parrish, D. D., Ziemke, J., Balashov, N. V., Cupeiro, M., Galbally, I. E., Gilge, S., Horowitz, L., Jensen, N. R., Lamarque, J.-F., Naik, V., Oltmans, S. J., Schwab, J., Shindell, D. T., Thompson, A. M., Thouret, V., Wang, Y., and Zbinden, R. M.: Global distribution and trends of tropospheric ozone: An observation-based review, Elementa: Science of the Anthropocene, 2, 2014.
- De Maziere, M., Thompson, A. M., Kurylo, M. J., Wild, J. D., Bernhard, G., Blumenstock, T., Braathen, G. O., Hannigan, J. W., Lambert, J.-C., Leblanc, T., McGee, T. J., Nedoluha, G., Petropavlovskikh, I., Seckmeyer, G., Simon, P. C., Steinbrecht,W., and Strahan, S. E.: The Network for the Detection of Atmospheric Composition Change (NDACC): history, status and perspectives, Atmospheric Chemistry and Physics, 18, 4935–4964, https://doi.org/10.5194/acp-18-4935-2018, 2018.
- Farman, J. C., Gardiner, B. G., and Shanklin, J. D.: Large losses of total ozone in Antarctica reveal seasonal ClOx/NOx interaction, Nature, 315, 207–210, https://doi.org/10.1038/315207a0, 1985.
- Fioletov, V., Zhao, X., Abboud, I., Brohart, M., Ogyu, A., Sit, R., Lee, S. C., Petropavlovskikh, I., Miyagawa, K., Johnson, B. J., Cullis, P., Booth, J., McConville, G., and McElroy, C. T.: Total ozone

variability and trends over the South Pole during the wintertime, Atmospheric Chemistry and Physics, 23, 12 731–12 751, https://doi.org/10.5194/acp-23-12731-2023, 2023.
- Fioletov, V. E., Kerr, J. B., McElroy, C. T.,Wardle, D. I., Savastiouk, V., and Grajnar, T. S.: The Brewer reference triad, Geophysical Research Letters, 32, https://doi.org/https://doi.org/10.1029/2005GL024244, 2005.
- Garcia, O. E., Schneider, M., Hase, F., Blumenstock, T., Sepulveda, E., and Gonzalez, Y.: Quality assessment of ozone total column amounts as monitored by ground-based solar absorption spectrometry in the near infrared (> 3000 cm-1), Atmospheric Measurement Techniques, 7, 3071–3084, https://doi.org/10.5194/amt-7-3071-2014, 2014.
- Godin-Beekmann, S., Azouz, N., Sofieva, V. F., Hubert, D., Petropavlovskikh, I., Effertz, P., Ancellet, G., Degenstein, D. A., Zawada, D., Froidevaux, L., Frith, S., Wild, J., Davis, S., Steinbrecht, W., Leblanc, T., Querel, R., Tourpali, K., Damadeo, R., Maillard Barras, E., Stubi, R., Vigouroux, C., Arosio, C., Nedoluha, G., Boyd, I., Van Malderen, R., Mahieu, E., Smale, D., and Sussmann, R.: Updated trends of the stratospheric ozone vertical distribution in the 60◦ S–60◦ N latitude range based on the LOTUS regression model, Atmospheric Chemistry and Physics, 22, 11 657–11 673, https://doi.org/10.5194/acp-22-11657-2022, 2022.
- Gordon, I., Rothman, L., Hargreaves, R., Hashemi, R., Karlovets, E., Skinner, F., Conway, E., Hill, C., Kochanov, R., Tan, Y., Wcisło, P., Finenko, A., Nelson, K., Bernath, P., Birk, M., Boudon, V., Campargue, A., Chance, K., Coustenis, A., Drouin, B., Flaud, J., Gamache, R., Hodges, J., Jacquemart, D., Mlawer, E., Nikitin, A., Perevalov, V., Rotger, M., Tennyson, J., Toon, G., Tran, H., Tyuterev, V., Adkins, E., Baker, A., Barbe, A., Cane, E., Csaszar, A., Dudaryonok, A., Egorov, O., Fleisher, A., Fleurbaey, H., Foltynowicz, A., Furtenbacher, T., Harrison, J., Hartmann, J., Horneman, V., Huang, X., Karman, T., Karns, J., Kassi, S., Kleiner, I., Kofman, V., Kwabia–Tchana, F., Lavrentieva, N., Lee, T., Long, D., Lukashevskaya, A., Lyulin, O., Makhnev, V., Matt, W., Massie, S., Melosso, M., Mikhailenko, S., Mondelain, D., Muller, H., Naumenko, O., Perrin, A., Polyansky, O., Raddaoui, E., Raston, P., Reed, Z., Rey, M., Richard, C., Tobias, R., Sadiek, I., Schwenke, D., Starikova, E., Sung, K., Tamassia, F., 725 Tashkun, S., Vander Auwera, J., Vasilenko, I., Vigasin, A., Villanueva, G., Vispoel, B.,Wagner, G., Yachmenev, A., and Yurchenko, S.: The HITRAN2020 molecular spectroscopic database, Journal of Quantitative Spectroscopy and Radiative Transfer, 277, 107 949, https://doi.org/https://doi.org/10.1016/j.jqsrt.2021.107949, 2022.
- Haigh, J. D. and Pyle, J. A.: Ozone perturbation experiments in a two-dimensional circulation model, Quarterly Journal of the Royal Meteorological Society, 108, 551–574, https://doi.org/https://doi.org/10.1002/qj.49710845705, 1982.
- Hannigan, J., Palm, M., Jones, N., Ortega, I., Langerock, B., Mahieu, E., Zhou, M., and Smale, D.: SFIT4 Line-by-line nonlinear spectral fitting software: version 1.0.18, https://doi.org/10.18758/ZEI21098, 2024.
- Harris, N. R. P., Ancellet, G., Bishop, L., Hofmann, D. J., Kerr, J. B., McPeters, R. D., Prendez, M., Randel, W. J., Staehelin, J., Subbaraya, B. H., Volz-Thomas, A., Zawodny, J., and Zerefos, C. S.: Trends in stratospheric and free tropospheric ozone, Journal of Geophysical Research: Atmospheres, 102, 1571–1590, https://doi.org/https://doi.org/10.1029/96JD02435
- , 1997.
- Hase, F., Hannigan, J., Coffey, M., Goldman, A., Hopfner, M., Jones, N., Rinsland, C., and Wood, S.: Intercomparison of retrieval codes used for the analysis of high-resolution, ground-based FTIR measurements, Journal of Quantitative Spectroscopy and Radiative Transfer, 87, 25–52, https://doi.org/https://doi.org/10.1016/j.jqsrt.2003.12.008, 2004.
- Hoinka, K. P., Claude, H., and Kohler, U.: On the correlation between tropopause pressure and ozone above central Europe, Geophysical Research Letters, 23, 1753–1756, https://doi.org/https://doi.org/10.1029/96GL01722, 1996.
- IASI: IASI portal, Atmospheric composition data products, https://iasi.aeris-data.fr/, accessed: 2025-10-20, 2025.

- Inness, A., Ades, M., Agusti-Panareda, A., Barre, J., Benedictow, A., Blechschmidt, A.-M., Dominguez, J. J., Engelen, R., Eskes, H., Flemming, J., Huijnen, V., Jones, L., Kipling, Z., Massart, S., Parrington, M., Peuch, V.-H., Razinger, M., Remy, S., Schulz, M., and Suttie, M.: The CAMS reanalysis of atmospheric composition, Atmospheric Chemistry and Physics, 19, 3515–3556, https://doi.org/10.5194/acp-19-3515-2019, 2019.
- IRWG: Infrared Working Group, https://www2.acom.ucar.edu/irwg, accessed: 2025-11-17, 2025.
- Jonassen, M. O., Chechin, D., Karpechko, A., Lupkes, C., Spengler, T., Tepstra, A., Vihma, T., and Zhang, X.: Dynamical Processes in the Arctic Atmosphere, pp. 1–51, Springer International Publishing, Cham, https://doi.org/10.1007/978-3-030-33566-3_1, 2020.
- Keppens, A., Hubert, D., Granville, J., Nath, O., Lambert, J.-C., Wespes, C., Coheur, P.-F., Clerbaux, C., Boynard, A., Siddans, R., Latter, B., Kerridge, B., Di Pede, S., Veefkind, P., Cuesta, J., Dufour, G., Heue, K.-P., Coldewey-Egbers, M., Loyola, D., Orfanoz-Cheuquelaf, A., Maratt Satheesan, S., Eichmann, K.-U., Rozanov, A., Sofieva, V. F., Ziemke, J. R., Inness, A., Van Malderen, R., and Hoffmann, L.: Harmonisation of sixteen tropospheric ozone satellite data records, Atmospheric Measurement Techniques, 18, 6893–6916, https://doi.org/10.5194/amt-18-6893-2025, 2025.
- Kivi, R., Kyro, E., Turunen, T., Harris, N. R. P., von der Gathen, P., Rex, M., Andersen, S. B., and Wohltmann, I.: Ozonesonde observations in the Arctic during 1989–2003: Ozone variability and trends in the lower stratosphere and free troposphere, Journal of Geophysical Research: Atmospheres, 112, https://doi.org/https://doi.org/10.1029/2006JD007271, 2007.
- Langematz, U., Tully, M. B., Calvo, N., Dameris, M., de Laat, A. T. J., Klekociuk, A., Muller, R., and Young, P.: Polar Stratospheric Ozone: Past, Present, and Future, in: Scientific Assessment of Ozone Depletion: 2018, Global Ozone Research and Monitoring Project – Report No. 58, chap. 4, World Meteorological Organization / UNEP, Geneva, Switzerland, https://wmo.int/scientific-assessment-of-ozone-depletion-2018, last accessed: 02/12/2025, 2018.
- Law, K. S., Hjorth, J. L., Pernov, J. B., Whaley, 760 C. H., Skov, H., Collaud Coen, M., Langner, J., Arnold, S. R., Tarasick, D., Christensen, J., Deushi, M., Effertz, P., Faluvegi, G., Gauss, M., Im, U., Oshima, N., Petropavlovskikh, I., Plummer, D., Tsigaridis, K., Tsyro, S., Solberg, S., and Turnock, S. T.: Arctic Tropospheric Ozone Trends, Geophysical Research Letters, 50, e2023GL103 096, https://doi.org/https://doi.org/10.1029/2023GL103096, e2023GL103096 2023GL103096, 2023.
- Millan, L., Hoor, P., Hegglin, M. I., Manney, G. L., Jeffery, P. S., Weyland, F. M., Leblanc, T., Walker, K. A., Boenisch, H., Kunkel, D., Petropavlovskikh, I., and Ye, H.: Ozone Trends in the Upper Troposphere-Lower Stratosphere Using Equivalent Latitude-Potential Temperature Coordinates, Geophysical Research Letters, 52, e2025GL118 651, https://doi.org/https://doi.org/10.1029/2025GL118651, e2025GL118651 2025GL118651, 2025.
- Mader, J. A., Staehelin, J., Brunner, D., Stahel, W. A., Wohltmann, I., and Peter, T.: Statistical modeling of total ozone: Selection of appropriate explanatory variables, Journal of Geophysical Research: Atmospheres, 112, https://doi.org/https://doi.org/10.1029/2006JD007694, 770 2007.
- Nilsen, K., Kivi, R., Laine, M., Poyraz, D., Van Malderen, R., von der Gathen, P., Tarasick, D. W., Tholix, L., and Jepsen, N.: Time-varying trends from Arctic ozonesonde time series in the years 1994-2022, Scientific Reports, 14, 27 683, https://doi.org/10.1038/s41598-024-75364-7, 2024.
- Ozonecci: ESA Climate Change Initiative Ozone project, https://climate.esa.int/fr/projets/ozone/data/, accessed: 2025-08-27, 2025.
- Pazmino, A., Goutail, F., Godin-Beekmann, S., Hauchecorne, A., Pommereau, J.-P., Chipperfield, M. P., Feng, W., Lefevre, F., Lecouffe, A., Van Roozendael, M., Jepsen, N., Hansen,

G., Kivi, R., Strong, K., andWalker, K. A.: Trends in polar ozone loss since 1989: potential sign of recovery in the Arctic ozone column, Atmospheric Chemistry and Physics, 23, 15 655–15, https://doi.org/10.5194/acp-23-15655-2023, 2023.
- Petropavlovskikh, I., Godin-Beekmann, S., Hubert, D., Damadeo, R., Hassler, B., and Sofieva, V.: SPARC/IO3C/GAW Report on Long-term Ozone Trends and Uncertainties in the Stratosphere, Tech. rep., https://elib.dlr.de/126666/, 9th assessment report of the SPARC project, published by the International Project Office at DLR-IPA. also: GAW Report No. 241; WCRP Report 17/2018, 2019.
- Rex, M., Salawitch, R. J., von der Gathen, P., Harris, N. R. P., Chipperfield, M. P., and Naujokat, B.: Arctic ozone loss and climate change, Geophysical Research Letters, 31, https://doi.org/https://doi.org/10.1029/2003GL018844, 2004.
- Rodgers, C. D.: Inverse Methods for Atmospheric Sounding, WORLD SCIENTIFIC, https://doi.org/10.1142/3171, 2000.
- Santer, B. D., Thorne, P. W., Haimberger, L., Taylor, K. E., Wigley, T. M. L., Lanzante, J. R., Solomon, S., Free, M., Gleckler, P. J., Jones, P. D., Karl, T. R., Klein, S. A., Mears, C., Nychka, D., Schmidt, G. A., Sherwood, S. C., and Wentz, F. J.: Consistency of modelled and observed temperature trends in the tropical troposphere, International Journal of Climatology, 28, 1703–1722, https://doi.org/https://doi.org/10.1002/joc.1756, 2008.
- Sen, P. K.: Estimates of the Regression Coefficient Based on Kendall's Tau, Journal of the American Statistical Association, 63, 1379–1389, https://api.semanticscholar.org/CorpusID:122323572, 1968.
- Smit, H. and the O3S-DQA Panel: Guidelines for Homogenization of Ozonesonde Data, SI2N/O3S-DQA Activity as part of "Past Changes in the Vertical Distribution of Ozone Assessment", https://www.wccos-josie.org/en/o3s-dqa/, last accessed 19 November 2025, 2012.
- Smit, H. G. J., Poyraz, D., Van Malderen, R., Thompson, A. M., Tarasick, D. W., Stauffer, R. M., Johnson, B. J., and Kollonige, D. E.: New insights from the Julich Ozone Sonde Intercomparison Experiment: calibration functions traceable to one ozone reference instrument, Measurement Techniques, 17, 73–112, https://doi.org/10.5194/amt-17-73-2024, 2024.
- Smit, H. G. J., T. A. M. and the ASOPOS 2.0 Panel: Ozonesonde Measurement Principles and Best Operational Practices, https://library.wmo.int/idurl/4/57720, last accessed 19 november 2025, 2021.
- Sofieva, V. F., Szela¸g, M., Tamminen, J., Kyrola, E., Degenstein, D., Roth, C., Zawada, D., Rozanov, A., Arosio, C., Burrows, J. P., Weber, M., Laeng, A., Stiller, G. P., von Clarmann, T., Froidevaux, L., Livesey, N., van Roozendael, M., and Retscher, C.: Measurement report: regional trends of stratospheric ozone evaluated using the MErged GRIdded Dataset of Ozone Profiles (MEGRIDOP), Atmospheric Chemistry and Physics, 21, 6707–6720, https://doi.org/10.5194/acp-21-6707-2021, 2021.
- Steinbrecht, W., Claude, H., KoHler, U., and Hoinka, K. P.: Correlations between tropopause height and total ozone: Implications for longterm changes, , 103, 19,183–19,192, https://doi.org/10.1029/98JD01929, 1998.
- Tarasick, D. W., Davies, J., Smit, H. G. J., and Oltmans, S. J.: A re-evaluated Canadian ozonesonde record: measurements of the vertical distribution of ozone over Canada from 1966 to 2013, Atmospheric Measurement Techniques, 9, 195–214, https://doi.org/10.5194/amt-9-195-2016, 2016.
- Van Malderen, R., Thompson, A. M., Kollonige, D. E., Stauffer, R. M., Smit, H. G. J., Maillard Barras, E., Vigouroux, C., Petropavlovskikh, I., Leblanc, T., Thouret, V., Wolff, P., Effertz, P., Tarasick, D. W., Poyraz, D., Ancellet, G., De Backer, M.-R., Evan, S., Flood, V., Frey, M. M., Hannigan, J. W., Hernandez, J. L., Iarlori, M., Johnson, B. J., Jones, N., Kivi, R., Mahieu, E., McConville, G., Muller, K., Nagahama, T., Notholt, J., Piters, A., Prats, N., Querel, R., Smale, D., Steinbrecht, W., Strong, K., and Sussmann, R.: Global groundbased tropospheric ozone

measurements: reference data and individual site trends (2000–2022) from the TOAR-II/HEGIFTOM project, Chemistry and Physics, 25, 7187–7225, https://doi.org/10.5194/acp-25-7187-2025, 2025a.
- Van Malderen, R., Zang, Z., Chang, K.-L., Bjorklund, R., Cooper, O. R., Liu, J., Maillard Barras, E., Vigouroux, C., Petropavlovskikh, I., Leblanc, T., Thouret, V., Wolff, P., Effertz, P., Gaudel, A., Tarasick, D. W., Smit, H. G. J., Thompson, A. M., Stauffer, R. M., Kollonige, D. E., Poyraz, D., Ancellet, G., De Backer, M.-R., Frey, M. M., Hannigan, J. W., Hernandez, J. L., Johnson, B. J., Jones, N., Kivi, R., Mahieu, E., Morino, I., McConville, G., Muller, K., Murata, I., Notholt, J., Piters, A., Prignon, M., Querel, R., Rizi, V., Smale, D., Steinbrecht, W., Strong, K., and Sussmann, R.: Ground-based tropospheric ozone measurements: regional tropospheric ozone column trends from the TOAR-II/HEGIFTOM homogenized datasets, Atmospheric Chemistry and Physics, 25, 9905–9935, https://doi.org/10.5194/acp-25-9905-2025, 2025b.
- Vigouroux, C., De Mazière,M., Demoulin, P., Servais, C., Hase, F., Blumenstock, T., Kramer, I., Schneider,M.,Mellqvist, J., Strandberg, A., Velazco, V., Notholt, J., Sussmann, R., Stremme, W., Rockmann, A., Gardiner, T., Coleman, M., and Woods, P.: Evaluation of tropospheric and stratospheric ozone trends over Western Europe from ground-based FTIR network observations, Atmospheric Chemistry and Physics, 8, 6865–6886, https://doi.org/10.5194/acp-8-6865-2008, 2008.
- Vigouroux, C., Blumenstock, T., Coffey, M., Errera, Q., Garcia, O., Jones, N. B., Hannigan, J.W., Hase, F., Liley, B., Mahieu, E., Mellqvist, J., Notholt, J., Palm, M., Persson, G., Schneider, M., Servais, C., Smale, D., Tholix, L., and De Maziere, M.: Trends of ozone total columns and vertical distribution from FTIR observations at eight NDACC stations around the globe, Atmospheric Chemistry and Physics, 15, 2915–2933, https://doi.org/10.5194/acp-15-2915-2015, 2015.
- Vogler, C., Bronnimann, S., Staehelin, J., and Griffin, R. E. M.: Dobson total ozone series of Oxford: Reevaluation and applications, Journal of Geophysical Research: Atmospheres, 112, https://doi.org/https://doi.org/10.1029/2007JD008894, 2007.
- von der Gathen, P., Kivi, R.,Wohltmann, I., Salawitch, R. J., and Rex,M.: Climate change favours large seasonal loss of Arctic ozone, Nature Communications, 12, 3886, https://doi.org/10.1038/s41467-021-24089-6, 2021.
- Weatherhead, E. C., Bodeker, G. E., Fasso, A., Chang, K.-L., Lazo, J. K., Clack, C. T. M., Hurst, D. F., Hassler, B., English, J. M., and Yorgun, S.: Spatial Coverage of Monitoring Networks: A Climate Observing System Simulation Experiment, Journal of Applied Meteorology and Climatology, 56, 3211 – 3228, https://doi.org/10.1175/JAMC-D-17-0040.1, 2017.
- Weber, M.: Stability requirements of satellites to detect long-term stratospheric ozone trends based upon Monte Carlo simulations, Atmospheric Measurement Techniques, 17, 3597–3604, https://doi.org/10.5194/amt-17-3597-2024, 2024.
- Weber, M., Arosio, C., Coldewey-Egbers, M., Fioletov, V. E., Frith, S. M., Wild, J. D., Tourpali, K., Burrows, J. P., and Loyola, D.: Global total ozone recovery trends attributed to ozone-depleting substance (ODS) changes derived from five merged ozone datasets, Atmospheric Chemistry and Physics, 22, 6843–6859, https://doi.org/10.5194/acp-22-6843-2022, 2022.
- World Meteorological Organization: Scientific Assessment of Ozone Depletion: 2022, https://library.wmo.int/idurl/4/58360, full Report, 2023.
- Zhou, M., Wang, P., Langerock, B., Vigouroux, C., Hermans, C., Kumps, N., Wang, T., Yang, Y., Ji, D., Ran, L., Zhang, J., Xuan, Y., Chen, H., Posny, F., Duflot, V., Metzger, J.-M., and De Maziere, M.: Ground-based Fourier transform infrared (FTIR) O3 retrievals from the 3040 cm-1 spectral range at Xianghe, China, Atmospheric Measurement Techniques, 13, 5379–5394, https://doi.org/10.5194/amt-13-845 5379-2020, 2020.